CZECH UNIVERSITY OF LIFE SCIENCES PRAGUE

FACULTY OF ENVIRONMENTAL SCIENCES (FES)

Department of Water Resources and Environmental Modelling

HYSPLIT dispersion modeling system in ABL of Mt. Etna volcano region using meteorological data

Diploma thesis

Supervisor - prof. doc. Mgr. Marek Vach, Ph.D.
Author: Sarbojeet Bhowmick

DECLARATION.

I hereby declare that this thesis was carried out independently with the use of the cited literature and under the supervision and guidance of prof. doc. Mgr. Marek Vach, Ph.D.

In Prague, 31.12.2022 Sarbojeet Bhowmick

ACKNOWLEDGEMENT

I would like to express my heartfelt appreciation to my thesis supervisor prof. doc. Mgr. Marek Vach, Ph.D. for his willingness to accept and supervise my diploma thesis. His invaluable professional guidance, the materials and the measurement data provided guided me throughout this project. Despite your busy schedule, you took the time to go through this script and give some suggestions to enhance this thesis. It was a great privilege and honour to work and study under your guidance. I am extremely grateful for what you have offered me. Many thanks also go to the Head of Department of Environmental Modelling, Dean of Faculty of Environmental Sciences, faculty Staff and all the lecturers for their professional teaching. I wish to express my high gratitude to the delegated person involved in writing this thesis, prof. doc. Mgr. Marek Vach, Ph.D. He is very generous in sharing his knowledge in this thesis work. His extensive effort made this work executable and satisfactory. I would like to thank my beloved Dad and Mom for supporting me inevitably. My close friends and colleagues offered me deep insight into my thesis work and supported me directly or indirectly in my studies at the Czech University of Life Sciences, Prague.

God blessings.

In Prague, 31.12.2022 Sarbojeet Bhowmick

ABSTRACT

Hybrid Single-Particle Lagrangian Integrated Trajectory model (HYSPLIT), developed by National Oceanic and Atmospheric Administration (NOAA) Air Resources Laboratory, is one of the most extensive modelling system for Atmospheric Boundary Layer (ABL) trajectories and dispersion calculations. A 3-d Lagrangian based tool HYSPLIT uses meteorological data as input for the dispersion calculation. HYSPLIT support a variety of different meteorological data simulations. This work describes the results obtained from Volcanic ash transport and dispersion (VATD) models using HYSPLIT from NOAA satellite using GDAS Meteorological data of Mount Etna volcanic region . HYSPLIT interface programs which are generally available to process ETA, ECMWF, NOAA, Copernicus or other model output fields. This thesis highlights the HYSPLIT model simulation results of Mount Etna volcanic region specifying the volcanic ash deposition at different heights and, ash particle position of calculated areas. Simulation results includes the data of Mount Etna last year eruption on 16 February, 2021 reflects on VATD models with February and March month data set.

Keywords: Lagrangian; NOAA; HYSPLIT, VATD, GDAS, Mount Etna, volcanic ash, ash particle, simulation.

Table of Contents

LIST OF FIGURES

1. INTRODUCTION

Volcano observatories are relative in organizing under the banner of the World Organization of Volcano Observatories, a commission of the International Association of Volcanology and the Earth's Interior, which holds membership for the International Union of Geodesy and Geophysics. Not all volcanoes are monitored and not all countries have volcano observatories. Volcano observatory staff can detect volcanic unrest, provide eruption forecasts, identify the onset of an eruption, and advise on the evolution and end of an eruption. Ideally these volcano observatories provide guidance on the changing eruption characteristics through time such as plume heights, altitudes of dispersing ash layers in the atmosphere, likely particle size distribution (post initial eruption) and possible mass eruption rates that can be used in numerical dispersion and transport models. Many observatories may analyse eruption products providing information on composition of ash and also gas emissions that impact on aircraft systems. Volcano observatories typically also hold information on past eruptions of a given volcano so they are able to provide likely eruption scenarios and a range of likely eruption parameters, such as possible ash ejection heights, before an eruption occurs. They are also responsible for monitoring ground hazards such as ash fall and volcanic gas dispersal.

Researches proved that the atmospheric dispersion model HYSPLIT (Stein et al., 2015), already in use by Met Service for the movement of fine particles travelling in the atmosphere, such as volcanic ash, and found it has the capability for estimating the distribution of ash particles on the ground. As well as capturing the influence of realistic atmospheric motion in ash transport, HYSPLIT can also model in-cloud (rainout) and below-cloud (washout) wet deposition processes. HYSPLIT is a hybrid Lagrangian dispersion model, developed by NOAA/ARL which is used by MetService, in its role as a Volcanic Ash Advisory Centre (VAAC), to model airborne volcanic ash, with meteorological data provided by external and in-house NWP (Numerical Weather Prediction) models, which operate with three spatial dimensions and time. The spatial resolution of these models is four km, and the temporal resolution one hour. HYSPLIT is operationally used by several of the Volcanic Ash Advisory Centres for aviation forecasting. A by-product of the HYSPLIT volcanic ash dispersion simulations is the ash deposition at the ground surface. The ground surface elevation is modelled at the same resolution as the atmospheric model. Aside from the dispersion of volcanic ash, HYSPLIT is used in several other atmospheric transport applications, including the dispersion of hazardous materials (e.g. nuclear material after the Fukushima reactor accident), air quality modelling (e.g. ozone, visibility, haze, and dioxin), dust storms, smoke, and the transport of biological material (e.g. pollen and mould spores). Rather than using a horizontal dispersion coefficient, the dispersion was calculated from the friction velocity, height and boundary layer height, where there are different equations for stable/neutral and unstable layers for both the surface and boundary layer. Above the boundary layer a mixing coefficient obtained from mixing length theory is generally used to calculate the velocity variances. The ash deposition results from HYSPLIT obtained for similar eruptions and wind patterns. This showed that alterations to the standard fall velocity model of HYSPLIT were required to deal with ash particles larger than about 100 microns, which make up the bulk of ash deposits near a volcano. This is not a consideration in the aviation applications of HYSPLIT, as these particles are the ones that rapidly fall out of ash clouds.

2. OBJECTIVE

The goal of this work is based on classified results obtained from HYSPLIT Model using GDAS Meteorological data in Mount Etna volcanic region.
The assessments in the context of this work produced by HYSPLIT Model are basically focused on:

1. volcanic ash deposition and mass concentration;
2. ash particle position at different heights.

3. LITERATURE REVIEW

This part deliberates information regarding HYSPLIT model, overviews of Mount Etna volcano, and volcanic ash distribution in Planetary Boundary Layer (PBL) which will help us to find out the impact of HYSPLIT modelling working system.

3.1 LAGRANGIAN ANALYSIS

As provided by Gifford. (1982); de Baas et al. (1986); Sawford and Guest. (1987); Thomson. (1987); Luhar and Britter. (1989) and Yaping Shao (1991) the Lagrangian dispersion models brings outstanding predictions for the distributed of air pollutants in both homogeneous and inhomogeneous turbulent airflows. The Lagrangian dispersion model based in a simulation of tracer trajectories, naturally describe the movement of a pollutant and are numerically simple. Based on Thomson (1987) the Lagrangian model unfolds the characteristics on the movement of a passive particle in a turbulent flow which can be adequately described by a nonlinear stochastic equation system as follows:

$$dU_i = a_i dt + b_{ij} d\xi_j$$
$$dX_i = U_i dt \qquad \text{... (1)} \quad \text{(Yaping Shao, 1991)}$$

Here, U_i and X_i are the velocity and position of the particle, respectively; t is time; and $d\xi_j$ is a random acceleration. The coefficients a_i and b_{ij} are determined by the structure of turbulence.
Using this method a complete understanding of atmospheric turbulence over uniform surfaces has been achieved and this has provided a solid basis for the application of Lagrangian models. In this thesis, Lagrangian trajectory models have been obtained using HYSPLIT application.

3.1.1 Lagrangian particle trajectories in Atmospheric Boundary Layer (ABL)

High Reynolds-number turbulence is evaluated by intermittency in its small-scale structure, where the velocity gradients and the instantaneous turbulent kinetic energy (TKE) dissipation rate ϵ^* exhibit large fluctuations in time provided by Chen (1971). According to Andy M. Reynolds et al. (2018) Lagrangian models of tracer-particle trajectories in turbulent flows can be adapted for simulation of particle trajectories. This is conventionally done by replacing the zero mean fall speed of a tracer-particle with the terminal speed of the particle. Such models have been used widely to predict spore and pollen dispersal. In ABL flows, Pope (2000) proposed that intermittency in ϵ^* can play a significant role, where the ratio between ϵ^* and its time-averaged value (= ϵ) can reach as high as 50. However, in Lagrangian stochastic (LS) particle trajectory models have significant impact on the intermittent behaviour of ϵ^*. Thomson (1987); Wilson and Sawford (1996) studies shows that LS models typically do not consider for the intermittent behaviour of ϵ^*. LS models estimates a local Lagrangian time scale as a

function of a local ϵ (Flesch and Wilson 1992; Baldocchi 1997; Kurbanmuradov and Sabelfeld 2000; Rannik et al. 2000; Kljun et al. 2002; Nathan et al. 2002; Cassiani et al. 2005a,b; Poggi et al. 2006; Vesala et al. 2008; Hsieh and Katul 2009). Studies from Pope and Chen (1990) using an extended LS model that includes not only the instantaneous velocity, but also the instantaneous dissipation (ϵ^*) along a particle trajectory. In this model, where the dissipation rate ϵ^* is sampled from a log-normal probability density function (PDF), by solving an additional stochastic differential equation for $\chi \equiv \ln(\epsilon^*/\epsilon)$. In the Lagrangian frame of reference, Thomson (1987) formulated simplest two-dimensional case based on the generalized Langevin equation. According to T. Duman et al. (2014) based on standard LS model and proposed log-normal model simulations for ABL flows were observed as shown in Fig.1

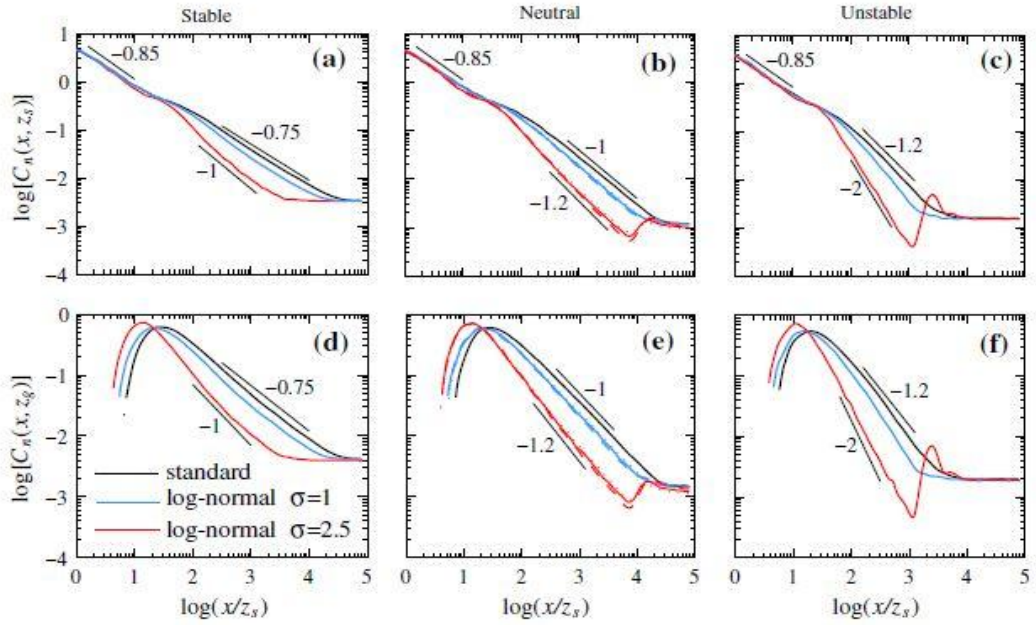

Fig. 1. Horizontal variation of normalized concentration as a function of distance from the source x for ABL flows. SI stands for source intensity and u_r is the wind velocity at source height. a–c plots shows the horizontal variation at the source height (z_s) for stable, neutral and unstable conditions respectively. d–f presents the same but at ground level (z_g). The solid lines in all sub-figures represent simulations with $C_\chi = 1.6$. For the neutral case (b, e), simulations of $C_\chi = 0.5$ and 3 shown by the dashed lines and the dotted lines respectively (T. Duman et al., 2014)

According to Alam and Lin (2008) in an atmospheric model, a set of conservation principles form a coupled set of PDEs that must be solved simultaneously. A system of prognostic equations describing atmospheric motion can be compactly written as

$$\frac{d\Psi}{dt} + \text{u. d}\Psi = \text{R} \qquad \text{... (2) (Alam and Lin, 2008)}$$

Here, Ψ is a vector of d state variables, u is a two or three-dimensional velocity vector, and R is a vector that represents all forces or sources. In the absence of external forces or source/sink terms: R = 0, which implies that

$$\frac{d\Psi}{dt} = 0 \quad \text{...(3)}$$

In Lagrangian models, in the first stage of the time step we can assume that an atmospheric state is governed by inertial forces only. Therefore, an air parcel in motion moves with the current velocity without changing Ψ within the parcel. In the second stage of the time step, we neglect the motion of air parcels and consider that an

atmospheric state is at rest, where flow properties defined by Ψ changes within a parcel according to external sources/sinks or forces represented by nonzero R. For example, such movement of air parcels shown below in Fig.2.

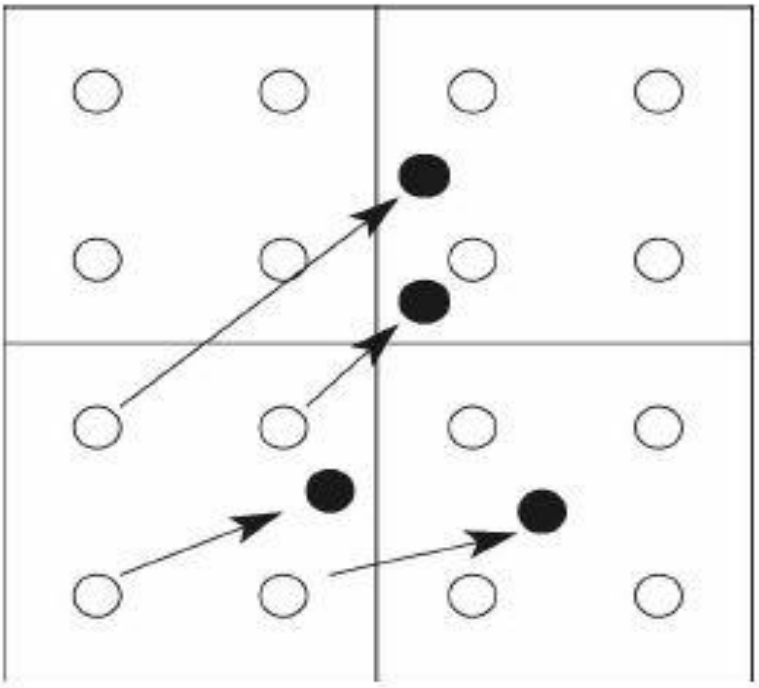

Fig. 2. Movement of parcels in a typical two-dimensional model is presented schematically. A non-filled circle represents a parcel assigned at $t \rightarrow t_0$. A filled circle represents a parcel at $t = t_0 + \Delta t$. Arrows link present position with future positions. (Alam and Lin , 2008)

Studies from Robert G. Lamb (1977) mentions the ensemble mean concentration of a passive, chemically inert species of air particles using Lagrangian equation. The results observed from the simulations are of mean particle height, root-mean-square vertical and lateral spread and mean cross-wind integrated concentrations estimated using Willis and Deardorff (1978) boundary model. Dosio, A., & De Arellano, J. V. (2006) approaches the Lagrangian statistics in the Convective Boundary Layer (CBL) using Large Eddy Simulation (LES), i.e. trajectories of particles released in a numerically generated turbulent flow are tracked in space and time. Author examined three main issues using LES as follows: First, the turbulent characteristics of the flow have been studied in both Eulerian and Lagrangian frameworks by analyzing velocity auto correlations and calculating integral scales. Second, the relationship between flow properties (auto correlations) and dispersion characteristics (particles displacements) which have been discussed through Taylor's analysis of turbulent dispersion provided by Taylor (1921). The influence of the asymmetry of the CBL flow on dispersion is studied, with the focus being on the difference between horizontal and vertical motion. And, finally the relationship between Eulerian and Lagrangian frameworks is studied by calculating the ratio β between the Lagrangian and Eulerian time scales. Lagrangian particle model analyzed using the position in direction j of the i^{th} particle calculated using the equation:

$$x_j^i(t+\Delta t) = x_j^i(t) + u_j^i(t)\Delta t \quad \ldots(4)$$ (Dosio, A., & De Arellano, J. V., 2006)

Here, Δt is the time step and $u_j^i(t)$ is the velocity of the particle calculated by interpolating linearly the values of the resolved (Eulerian) velocity at the eight closest

grid points. In contrary, Lagrangian statistics (both auto correlations and integral scales) are associated with the largest scale of motion, which were explicitly solved by the LES and therefore the velocity sub grid scales are not very relevant. Lagrangian auto correlation for both the horizontal and vertical components were calculated at different heights as shown below in Fig. 3.

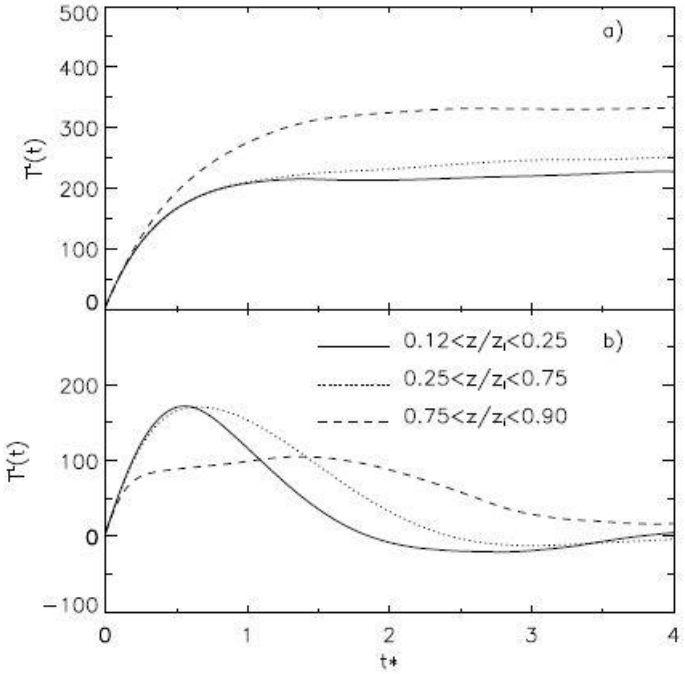

Fig. 3. Lagrangian Integral of the auto correlation for the horizontal (a) and vertical (b) wind components for particles released at different heights. (Dosio, A., & De Arellano, J. V., 2006)

In Fig.4, according to Lagrangian statistics an example of particle trajectory is shown. According to Moeng and Sullivan (1994), the difference in the particle motions at short times is related to the different vertical structure of the turbulent field in the CBL.

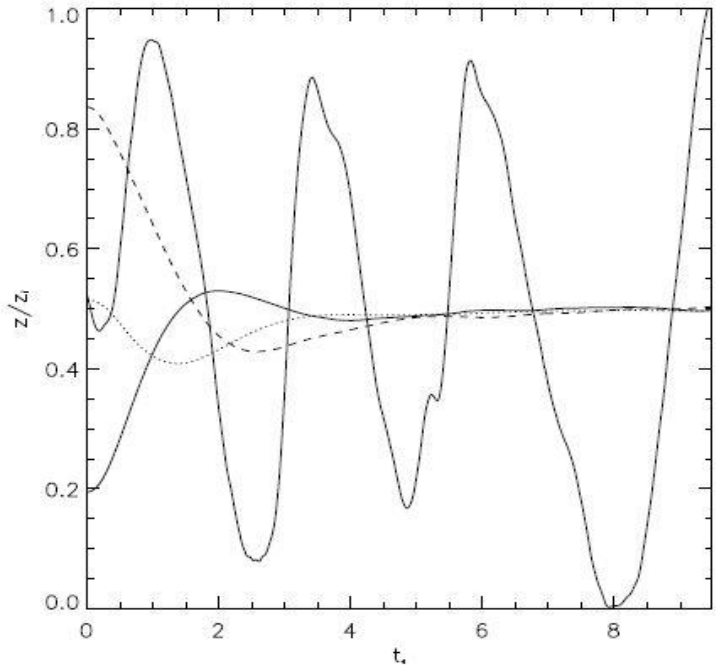

Fig. 4. Mean plume height (plume center line) of particles released at three different heights (Dosio, A., & De Arellano, J. V., 2006)

This thesis works with the volcanic ash particle trajectories using Lagrangian statistics as mentioned in this section. The volcanic ash particle trajectories based on Alam and Lin (2008) equations (2) and, (3) respectively follows in this thesis work using HYSPLIT model application of Mount Etna volcanic ash particle position and trajectories.

3.1.2 Overview of volcanic ash particle trajectories

Studies from Ram and Gayley (1991) ensures that volcano eruptions often release volcanic ash clouds into the atmosphere, which consist of tephra (submillimeter-sized rock particles), water vapor and other gases such as carbon dioxide (CO_2), sulfur dioxide (SO_2), hydrogen sulfide (H_2S), etc. Ash particles from volcano eruptions are transported by wind to thousands of kilometers away, or even over 10,000 km from their source for some fine particles. Volcanic ash plumes can reach over 20 km in altitude above sea level provided by Holasek et al., (1996).

According to T. Haszpra and T. Tél (2011), the equations of motion for small, inertial, spherical particles of radius r in a viscous fluid advected by a flow deterministically are given by the Maxey-Riley equations (Studies by M. Farazmand and G. Haller (2014)). For heavy particles of density ρ_p much larger than that of the ambient medium ρ, the dimensionless equations for the particles trajectory $r_p(t)$ as follows:

$$\ddot{\mathbf{r}}_p = \frac{1}{St}\left(\mathbf{v}(\mathbf{r},t) - \dot{\mathbf{r}_p} - W_{terminal}\mathbf{n}\right)$$

…(5) T. Haszpra and T. Tél (2011)

where, v(r, t) is the flow field, $W_{terminal}$ is the dimensionless terminal velocity in still fluid, and n is a unit vector pointing upwards. Velocity and distance are measured in units of a characteristic velocity U and L, respectively. The Stokes number (St) appearing here is the dimensionless relaxation time of inertial particles subject to Stokes drag. Usually, the limit of $St \to 0$ in (5) implies finite acceleration only if the parentheses on the right hand side vanishes, the large-scale equation of motion for aerosol particles becomes even simpler than (5). On the contrary, the inertial effects are negligible, but in the vertical direction deposition has to be taken into account with a terminal velocity.

The dimensional equation of motion for volcanic ash particles following from (5) can be written as:

$$\mathbf{v}_p \equiv \dot{\mathbf{r}}_p = \mathbf{v}(\mathbf{r}_p(t),t) - w_{terminal}\mathbf{n}.$$

…(6) T. Haszpra and T. Tél (2011)

Here the $w_{terminal}$, the terminal velocity can be written as:

$$w_{terminal} = \frac{2}{9}r^2\frac{\rho_p}{\rho\nu}g.$$

…(7) T. Haszpra and T. Tél (2011)

According to Fay et al. (1995), the particle dispersion equations are formulated in terms of the turbulent velocity components. These velocity components are a function of the turbulent diffusivities computed in the previous section. In the particle implementation of the model, the dispersion process is represented by adding a turbulent component to the mean velocity

obtained from the meteorological data. The particle model can be applied in either the vertical, horizontal, or both directions. In this thesis the VATD models for ash particles deposition referred to as grain-sizr distributions (GSDs).
Studies from Draxler, R. R., & Hess, G. D. (1997) deliberates that the Puff dispersion model for ash particles is treated in two domains, when the puff is smaller than the meteorological model grid size and the other is larger. In the latter case it is assumed that the meteorological model is capable of resolving turbulent motions on that scale. GSDs and "top-hat" puffs are treated almost identically.
GSD distributions may be defined in either the vertical and horizontal directions, or only in the horizontal direction. For each GSD, concentrations are summed at each time step to all grid points that fall within the particle extent defined for GSD distributions ($\pm 1.54\ \sigma_i$), where i indicates z or h, or Gaussian distributions ($\pm 3.0\ \sigma_h$). Vertical distributions are always defined as top-hat while horizontal distributions may be either. The incremental concentration contribution by each GSD of mass m to a grid point is computed as follows:

$$\Delta c = m\ (\pi\ r^2\ \Delta z)^{-1} \quad \ldots(8)$$ Draxler, R. R., & Hess, G. D. (1997)

where the vertical extent $\Delta z = 3.08\sigma_z$, and the horizontal radius $r = 1.54\sigma_h$. All grid-nodes within the GSD extent receive the same Δc.
Particle calculations can be performed in either the vertical or both the vertical and horizontal directions. However, particle calculations are summed into a grid-cell rather than computed at a grid-point. A cell is defined at the center of the node and has an area corresponding to the half-way distance to adjacent nodes. The incremental concentration contribution to a cell by a single particle of mass m is defined for a 3D particle,

$$\Delta c = m\ (\Delta x\ \Delta y\ \Delta z)^{-1} \quad \ldots(9)$$ Draxler, R. R., & Hess, G. D. (1997)

Here, $\Delta x, \Delta y, \Delta z$ are the grid-cell dimensions. For every particle with a horizontal GSD the incremental concentration is same as equation (8), but with Δz defined as grid-cell height. If the horizontal distribution is Gaussian then the incremental concentration is the same as incremental concentration contribution for a Gaussian GSD, and with Δz defined as the grid-cell height. The incremental concentrations are added to each grid cell with each advection time step for all particles that intersect that point. The final average concentration is the incremental sum divided by the number of time steps in the concentration averaging period.

3.2 MOUNT ETNA

Mount Etna, a stratovolcano in Italy is the highest volcano in Europe and one of most active of the world. Located at 37° 45′ 18″ N, 14° 59′ 42″ E it's size is more than 3327 meters high with an average basal diameter of 40 km. Studies regarding endangerment of Mt. Etna began in the late 1970s and early 1980s focusing on the patterns in historic eruptions and speculating the location of future activity (Frazzetta and Romano, 1978; Guest and Murray, 1979; Duncan et al., 1981). Numerous studies have built on this work by statistics of historic eruptions (Mulargia et al., 1985; Behncke and Neri, 2003; Branca and Del Carlo, 2004, 2005; Salvi et al., 2006; Neri et al., 2011; Smethurst et al., 2009; Passarelli et al., 2010; Proietti et al., 2011) and making probabilistic hazard maps of surrounding areas (Andronico and Lodato, 2005; Bisson et al., 2009; Behncke et al., 2005; Crisci et al., 2010; Harris et al., 2011; Cappello et al., 2012, 2013).

Fig.5. Mount Etna (Source: wikipedia)

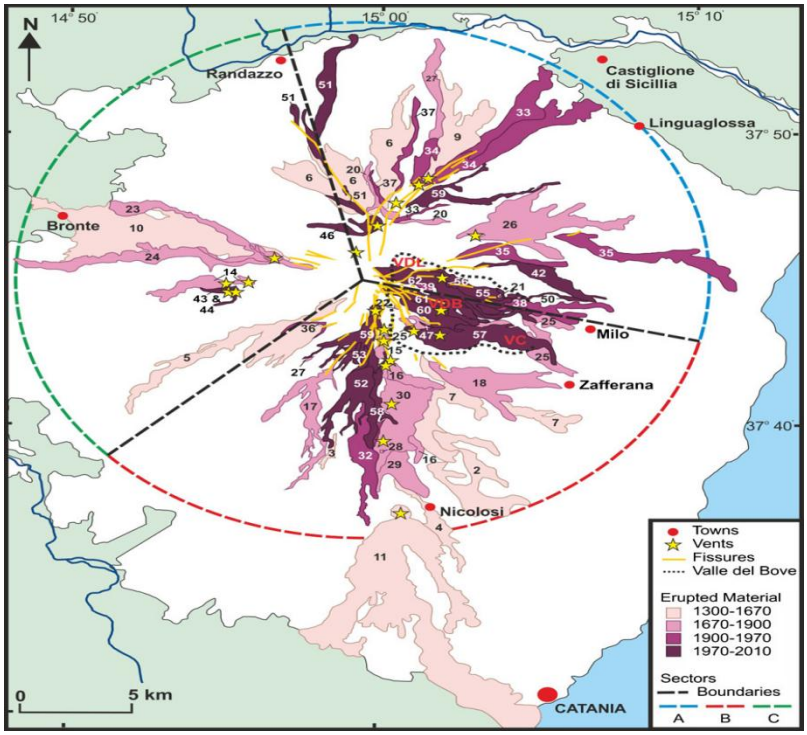

Fig.6. Sketch map of Mount Etna showing the extent of erupted material and the position of their vents or fissures (L.S. Gunn et al., 2014)

3.2.1 Importance of Mount Etna

Mount Etna, in June 2013 have been added to UNESCO World Heritage Site. Mount Etna, Latin Aetna, Sicilian Mongibello, active volcano on the east coast of Sicily. The name comes from the Greek Aitne, from aithō, "I burn." Mount Etna is the highest active volcano in

Europe, its topmost elevation being about 10,900 feet (3,320 metres). Like other active volcanoes, it varies in height, increasing from deposition during eruptions and decreasing from the periodic collapse of the crater′s rim. In 1865 the volcanic summit was about 170 feet (52 metres) higher than it was in the early 21st century. Etna covers an area of some 600 square miles (1,600 square km), and its base has a circumference of about 93 miles (150 km). About 35,000 to 15,000 years ago Etna experienced highly explosive eruptions generating large pyroclastic flows leaving extensive ignimbrite deposits. There are two types of volcanic activity which have been recognized in the historical records of Mt. Etna: persistent activity from summit vents and periodic activity from eruptive fissures on the volcano′s flanks (Guest and Murray 1979; Duncan et al., 1981; Acocella and Neri, 2003; Behncke and Neri, 2003; Branca and Del Carlo, 2005; Crisci et al., 2010). The Etna mountain has three ecological zones, one above the other, each exhibiting its own characteristic vegetation. The lowest zone, sloping gradually upward to perhaps 3,000 feet (915 metres), is fertile and rich in vineyards, olive groves, citrus plantations, and orchards. Several densely populated settlements, notably the city of Catania, are found on the lower slopes, but settlements become less frequent as the height increases. Above, the mountain grows steeper and is covered with forests of chestnut, beech, oak, pine, and birch. At heights of more than 6,500 feet (1,980 metres), the mountain is covered with ashes, sand, and fragments of lava and slag; there are a few scattered plants such as Astragalus aetnensis (local name: spino santo), which typically forms bushes almost 1 yard (about 0.9 metre) high, while some alpine plants manage to survive even near the top. Algae have been found near the steam outlets at 9,800 feet (2,990 metres) (Britannica web.).

Geologically, the Mount Etna indicates active signs since the end of the Neogene Period (i.e., for about the past 2.6 million years). The volcano has more than one active centre. A number of subsidiary cones have been formed on lateral fissures extending out from the centre and down the sides. The present structure of the mountain is the result of the activity of at least two main eruptive centers. The eruption of 1971 threatened several villages with its lava flow and destroyed some orchards and vineyards. Activity was almost continuous in the decade following 1971, and in 1983 an eruption that lasted four months prompted authorities to explode dynamite in an attempt to divert lava flows. The major eruptions of the 20th century occurred in 1986 and in 1999. In the early 21st century a major eruption began in July 2001 and lasted several weeks. Beginning of February 2021, Mount Etna began a series of explosive eruptions, which had made an impact on nearby villages and cities, with volcanic ash and rock falling as far away as Catania. As of 12 March 2021, the volcano has erupted 11 times in three weeks. The eruptions have consistently sent ash clouds over 10 km (33,000 ft) into the air, closing Sicilian airports. This thesis work made with the data set measured from the 16 February, 2021 eruption of Mount Etna.

Fig. 7. Social media post from a local just after the eruption of Mount Etna volcano on 16th February, 2021 (Source: Firstpost)

3.2.2 Eruptions of Mount Etna and forecasting

The data set generally used in this thesis is from last year eruption of Mount Etna on 16 February, 2021. Since 1300s the dataset of flank eruptions are in record from the description of summit and flanked activities provided by Tanguy et al. (2007) and Neri et al. (2011). Mount Etna as one of the active volcano in the world where eruptions occur quite frequently. In 2001, for example there were sixteen eruptions occur in Mount Etna. Major 20th century eruptions occurred in 1949, 1971, 1979, 1981, 1983 and 1991–1993. In 1971, lava buried the Etna Observatory (built in the late 19th century), destroyed the first generation of the Etna cable-car, and seriously threatened several small villages on Etna's east flank. In March 1981, the town of Randazzo on the northwestern flank of Etna narrowly escaped destruction by unusually fast-moving lava flows. That eruption was remarkably similar to one in 1928 that destroyed Mascali. The 1991–1993 eruption saw the town of Zafferana threatened by a lava flow, but successful diversion efforts saved the town with the loss of only one building a few hundred metres from the town's margin. Initially, such efforts consisted of the construction of earth barriers built perpendicularly to the flow direction; it was hoped that the eruption would stop before the artificial basins created behind the barriers would be completely filled. Instead, the eruption continued, and lava surmounted the barriers, heading directly toward Zafferana. Shortly after the blasting, the rate of lava emission dropped, and during the remainder of the eruption (until 30 March 1993) the lava never advanced close to the town again. In 2002-2003, a much larger eruption threw up a huge column of ash that could easily be seen from space. Eruptions, in 2001, 2002–2003, and 2004–2005 had lasted 3 weeks, 3 months, and 6 months, respectively. Lava flows advanced 6.5 km during the first few days of this eruption but thereafter stagnated at many minor distances from the vents; during the last months of the eruption lava rarely advanced more than 1 km down slope. On 3 December 2015, an eruption occurred between 03:20 and 04:10 local time. The Voragine crater exhibited a lava fountain which reached 1 km (3,300 ft) in height, with an ash plume which reached 3 km (9,800 ft) in height. The activity continued with an ash plume that reached 7 km (23,000 ft) in height that forced Catania airport to shut down for a few hours. Volcanic gas emissions from this volcano are measured by a multi-component gas analyzer system, which detects pre-eruptive degassing of rising magmas, improving prediction of volcanic activity. An eruption on 24

December 2018, following a dyke intrusion at shallow depth, spewed ash into the air, forcing the closure of airspace around Mount Etna. Two days later, a magnitude 4.9 earthquake shook the town of Fleri and surrounding towns. Mount Etna began a series of explosive eruptions, which have had an impact on nearby villages and cities, with volcanic ash and rock falling as far away as Catania. In 2021, the volcano has erupted eleven times in three weeks. The eruptions have consistently sent ash clouds over 10 km (33,000 ft) into the air, closing Sicilian airports.

Fig. 8. Mount Etna activity at night (Source: INGV-CT)

Fig. 9. Lava flows from Mount Etna during one of summit eruptions in 2006 (Source: INGV-CT)

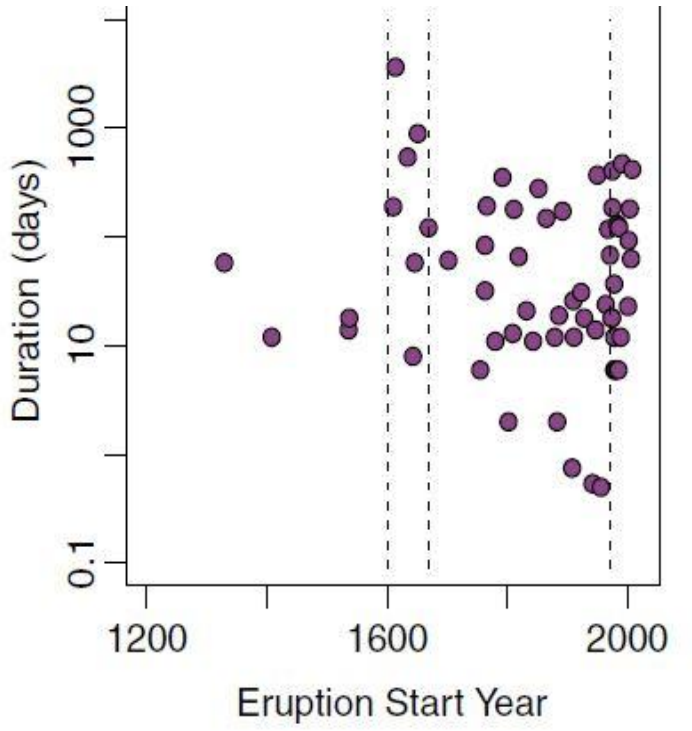

Fig. 10. Mount Etna cumulative eruption number (L.S. Gunn et al., 2014)

Mount Etna has a very long eruptive history that has been going on for over half a million years, but only in the last hundred thousand years has it assumed the conical shape that characterizes it today. The magma rises to the surface through an open central conduit that continuously releases the gaseous phases, generating the characteristic plume observable on the top of the volcano. National Institute of Geophysics and Volcanology - Catania section Istituto Nazionale di Geofisica e Vulcanologia (INGV-CT) responsible for the development and implement the system for forecasting volcanic plumes of Mount Etna. According to S. Scollo et al., (2009) forecasting performed by: a) downloading weather forecast data from meteorological mesoscale models; b) running models of tephra dispersal, c) plotting hazard maps of volcanic ash dispersal and deposition for certain scenarios and, d) publishing the results on a web-site dedicated to the Italian Civil Protection. Simulations are based on eruptive scenarios obtained by analysing field data collected from every Etna eruptions. Forecasting is supported by plume observations carried out by the monitoring system. Currently, the eruptive activity can be classified into three different categories:

- persistent activity : continuous degassing from the summit craters.

- terminal and sub terminal eruptions: lava eruptions that usually occur from the Summit Craters present on the top of the volcano (terminals) or from their immediate proximity (sub terminal).
- lateral and eccentric eruptions : occurs from eruptive vents that open along the slopes of the volcano, fed by magma that rises along the central duct (lateral eruptions), or through ducts independent from the central one (eccentric eruptions).

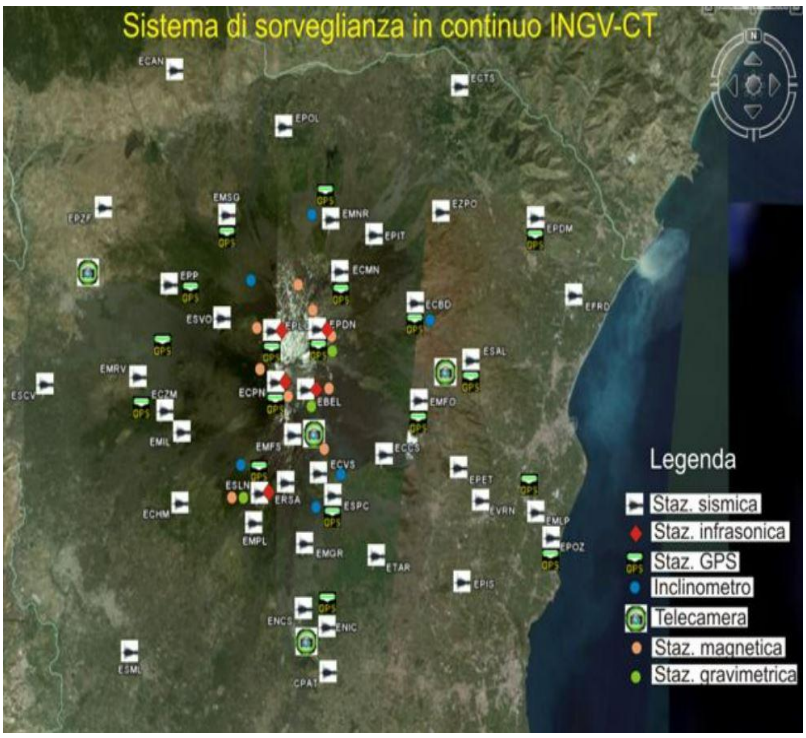

Fig. 11. Surveillance of Mount Etna by INGV-CT (Source: INGV-CT)

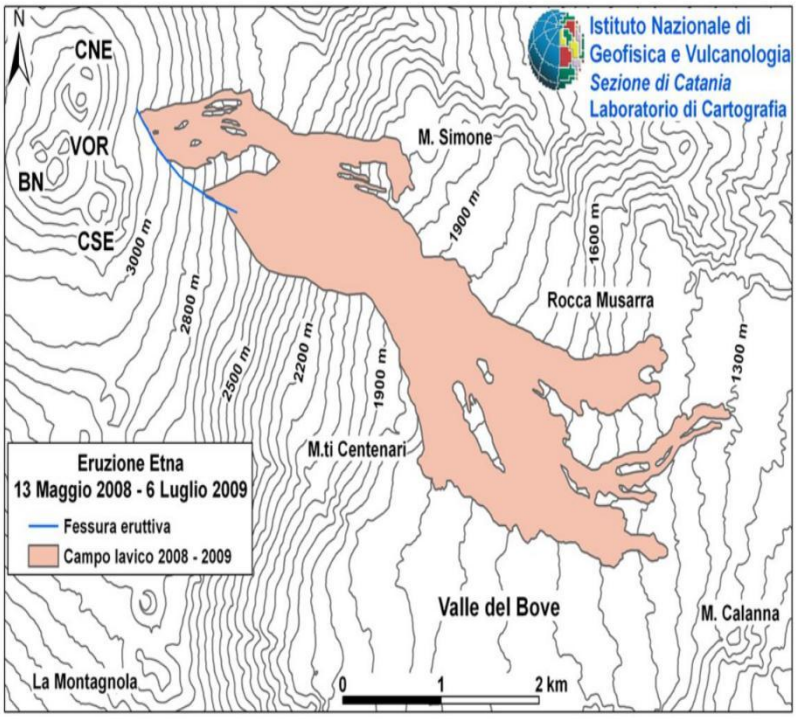

Fig. 12. Monitoring of Mount Etna eruptions between 2008-2009 (Source: INGV-CT)

The geochemical monitoring network was developed around 1984 to monitor all types of interactions present, in order to obtain, through the measurement of various parameters, a more complete picture of the state of activity of the volcano. Specifically, the network currently consists of thirteen stations for measuring the flow of CO_2 , the chemical-physical parameters of the aquifer and the TDGP and the temperatures of three fumaroles on the edge and internal wall of the La Fossa crater. Chemical-physical parameters of water and analysis of the chemical and isotopic composition of the water and gases dissolved in the groundwater through sampling carried out on a monthly basis. Monthly prospecting to estimate the diffuse

flow of CO_2 from the soils in three sectors of the Etna. The determination of the chemical and isotopic composition of the gases emitted in the peripheral and summit areas of the volcano. Bimonthly / monthly measurements for the analysis of the CO_2 / SO_2 ratios in the gases of the plume emitted by the Etna craters carries out.

3.3 VOLCANIC ASH TRANSPORT AND DISPERSION (VATD)

In this work VATD models obtained from HYSPLIT maintained by NOAA is a Lagrangian model and supports a wide range of simulations related to the transport, dispersion and deposition of substances in the air such as volcanic ash, radioactive species, smoke and dust. According to Peterson et al. (in press) they reflect on the different physical processes that effect the movement of volcanic ash particles, such as diffusion, settling and aggregation.

3.3.1 Volcanic ash deposition

Basaltic volcanism is the most widespread volcanic activity on Earth and also familiar to Mount Etna volcanic activity. Ash emissions are a very typical manifestation of basaltic activity despite of their frequency of occurrence. In this thesis, the volcanic ash concentration has been measured.The principal gases released during volcanic activity are water, carbon dioxide, hydrogen, sulfur dioxide, hydrogen sulfide, carbon monoxide and hydrogen chloride. The sulfur and halogen gases and metals are removed from the atmosphere by processes of chemical reaction, dry and wet deposition, and by adsorption onto the surface of volcanic ash. It has long been recognised that a range of sulfate and halide (primarily chloride and fluoride) compounds are readily mobilised from fresh volcanic ash. It is considered most likely that these salts are formed as a consequence of rapid acid dissolution of ash particles within eruption plumes, which is thought to supply the cations involved in the deposition of sulfate and halide salts. Studies provided by Taddeucci et al., (2002, 2004); Andronico et al., (2009a, 2013, 2014b) mentions the compositional features of ash particles erupted from explosive activity at Mount Etna. The Juvenile ash particles at Etna consist of two end-members: sideromelane and tachylite. The sideromelane has fluidal to irregular morphology, is yellow to brown in colour, transparent, vesicular and generally glassy in the groundmass. The tachylite is blocky, grey to black, generally opaque (sometimes it can be shiny), poorly vesicular and crystallised in the groundmass. Whereas, a continuous, progressive transition of textural features between the two ash types, mainly generated by the different extent of groundmass crystallisation, far more pronounced in tachylite, and by the higher content of (sub) spherical vesicles, as opposed to vesicles with complex and/or irregular shapes, in sideromelane. According to Taddeucci et al.,(2002, 2004); Polacci et al., (2006). In the 1995 eruption of Mount Etna , tachylite glass tends to be more compositionally differentiated in comparison to its sideromelane counterpart, with a higher silica, alkali and phosphorous content and lower magnesium and calcium. Studies by Taddeucci et al., (2004) proves that the eruptive activity investigations of ash componentry have revealed that the proportion of sideromelane ash increases with increasing eruption intensity. Ash dispersal at Mount Etna is mostly controlled by eruption intensity and the ensuing plume height. On 23 February and 23 November 2013, two lava fountain episodes characterised by relatively high eruption columns (atleast for the most common explosive activity at Etna) of up to 9–10 km a.s.l. and high MERs, generated dispersal of ash particles up to 400 km from Etna, in Puglia (Italy) studies by Poret et al., (2018a,b). During the 2001 and 2002–2003 eruptions the intensity was low but the duration of the activity last for days to weeks, the continuous injection of relatively fine-grained ash in the atmosphere is able to form a sustained tephra column feeding an eruption cloud spreading hundreds of kilometers away from the volcano. In this thesis, the volcanic ash deposition works with the ash concentration from volcanic plumes observed by the NOAA satellite.

3.3.2 Ash particle distribution

According to the work from M. Plu (2021), the 3-D representation of volcanic ash of a resolved source term and of the assimilation of different observation datasets, using the MOCAGE model. The main findings are as follows:

- The use of a resolved source term instead of a parameterised source term induces a more realistic representation of the horizontal dispersion of the ash plume.
- A positive impact of the assimilation of MODIS AOD on the horizontal dispersion of the plume has been shown, but this effect is rather low and local compared to source term improvement.
- The continuous assimilation of lidar profiles from two ground-based stations improves the vertical distribution of ash and helps to simulate ash concentrations closer to those values obtained from in situ observations.

According to Murrow et al., (1980); Carey and Sigurdsson (1982); Bonadonna and Houghton, (2005); Rose et al., (2007) grain size, the clayey material (VG) has a particle-size distribution between 1 and 200 μm with a maximum peak at around 20 μm and a second smaller, but wider, interval and a peak at 1500 μm. The volcanic ash (va) is almost unimodal and is characterized by coarser particles with a maximum peak at 150 μm, most of which are between 50 and 450 μm. The ash particles consist of tachylite. They show smoothed, poorly vesicular surfaces with conchoidal fractures. Webley et al. (2009) evaluated the sensitivity of the grain size distribution on the modeled ash cloud and found that this predefined distribution is sufficient for HYSPLIT volcanic ash simulation. In Rose (1993), the grain-size distribution of tephra produced during an eruption is highly relevant to aviation hazards but poorly characterized. Volcanic eruptions produce fragments ranging in size from meters to fractions of a micron. Particles larger than a millimeter or so fall out at roughly their terminal velocity and are generally removed from the eruption column in the first 30 min. Provided by Carey and Sigurdsson (1982), finer particles fall at rates influenced by variable and poorly understood processes of particle aggregation. The mass fraction of fine ash can be estimated from the total grainsize distribution (TGSD) of eruptive debris. Several studies have estimated the total grain-size distribution by analysis of old tephra deposits especially Suzuki et al., (1973); Walker, (1980); Sparks et al., (1981); Walker, (1981a,c); Self, (1983); Hayakawa, (1985); Woods and Bursik, (1991). The impact of explosive volcanic eruptions on climate and
air traffic strongly depends on the concentration and GSD of pyroclastic fragments injected into the atmosphere suggested by Girault et al., (2014). GSD is normally reconstructed by the volcanologists from grain size data at individual outcrops, ranging from basic unweighted average of the GSD at individual sparse outcrops to various integration methods of grain size data provided by Rose and Durant (2009). In volcanology, grain size distributions are given in terms of the ϕ, defined as $d = 2^{-\phi}$, where d is the particle diameter in mm. According to Heffter and Stunder (1993), the NOAA HYSPLIT GSD defines the particle bins as 1% total mass at 0.6 μm, 7% total mass at 2 μm, 25% of total mass at 6 μm and 67% of mass at 20 μm as originally used in the VATD. Vertically the volcanic ash distribution, i.e. the Height of ash $= \text{Max Height} - [Z_{width} \times P] + (0.5 \times Z_{width} \times R)$

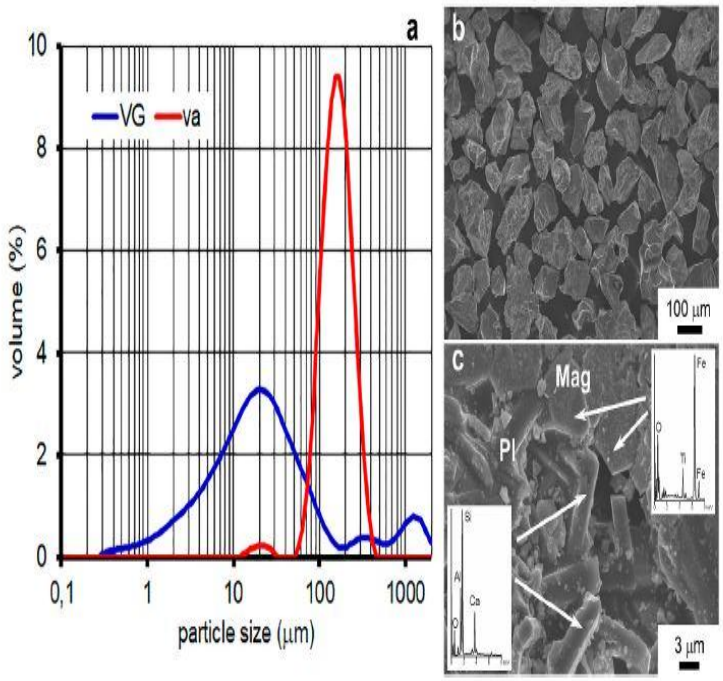

Fig. 13. Volcanic ash particle size from Mount Etna eruptions 2008-2009 (Source: INGV-CT)

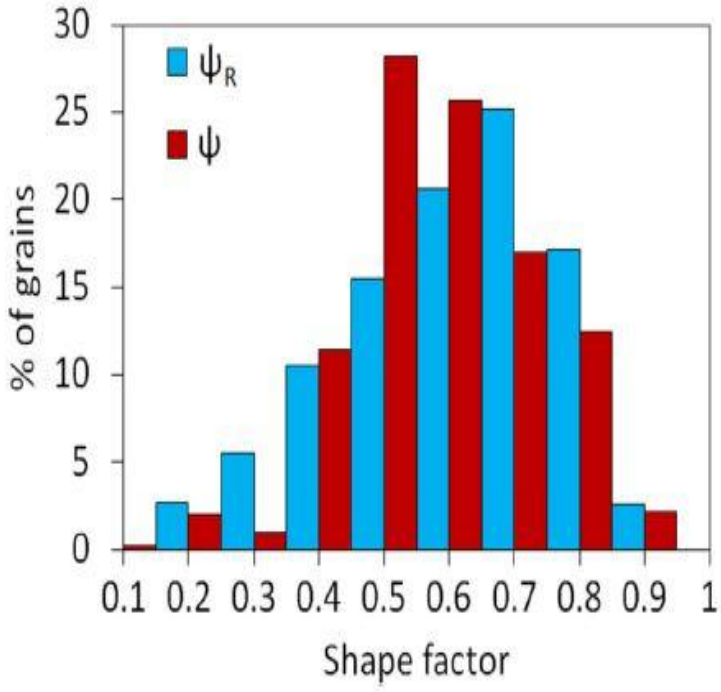

Fig. 14. Grain size distribution (in %) of ash particles in Mount Etna 2008 eruption (Source: INGV-CT)

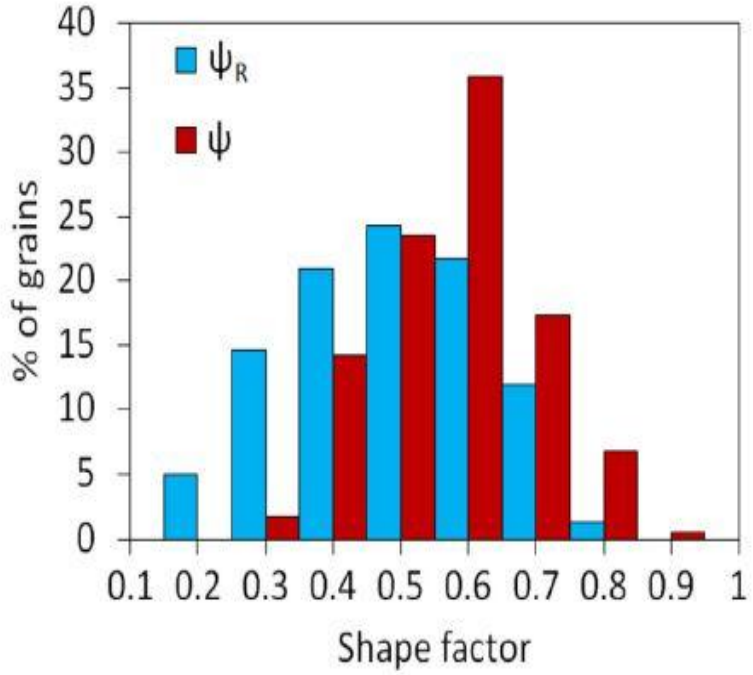

Fig. 15. Grain size distribution (in %) of ash particles in Mount Etna 2009 eruption (Source: INGV-CT)

3.4 HYSPLIT - A LAGRANGIAN BASED TOOL

According to the A.F. Stein et al., (2015) model calculation method is a hybrid between the Lagrangian approach, using a moving frame of reference for the advection and diffusion calculations as the trajectories or air parcels move from their initial location, and the Eulerian methodology, which uses a fixed three-dimensional grid as a frame of reference to compute pollutant air concentrations.

The HYSPLIT model has evolved throughout more than thirty years, from estimating simplified single trajectories based on radiosonde observations to a system accounting for multiple interacting pollutants. HYSPLIT can use a large variety of meteorological model data in its calculations, ranging from mesoscale to global scales. Rather than having a different version of HYSPLIT to cope with the variations in variables and structure for each meteorological data source, a customized preprocessor is used to convert each meteorological data source into a HYSPLIT-compatible format. In this way HYSPLIT can easily be run with one or more meteorological datasets at the same time, using the optimal data for each calculation point. The meteorological data already formatted for HYSPLIT that are publicly available from NOAA ARL website.

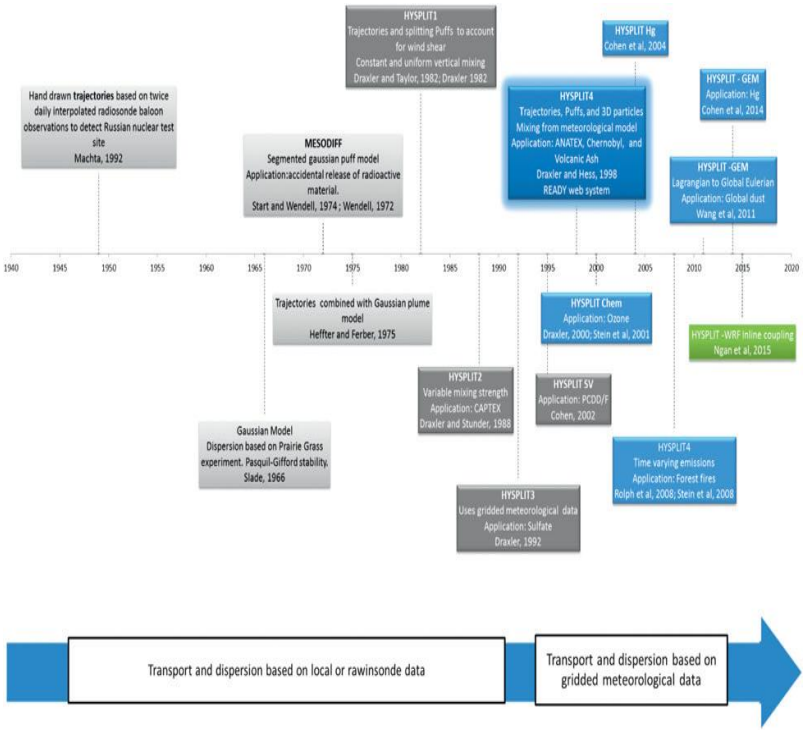

Fig. 16. Mechanism of the HYSPLIT model. The light gray shades leads HYSPLIT. The dark gray shade corresponds to the first three versions of the HYSPLIT system. The dark blue box corresponds to HYSPLIT4 and the light blue boxes correspond to applications that derive from HYSPLIT4. (A.F. Stein et al., 2015)

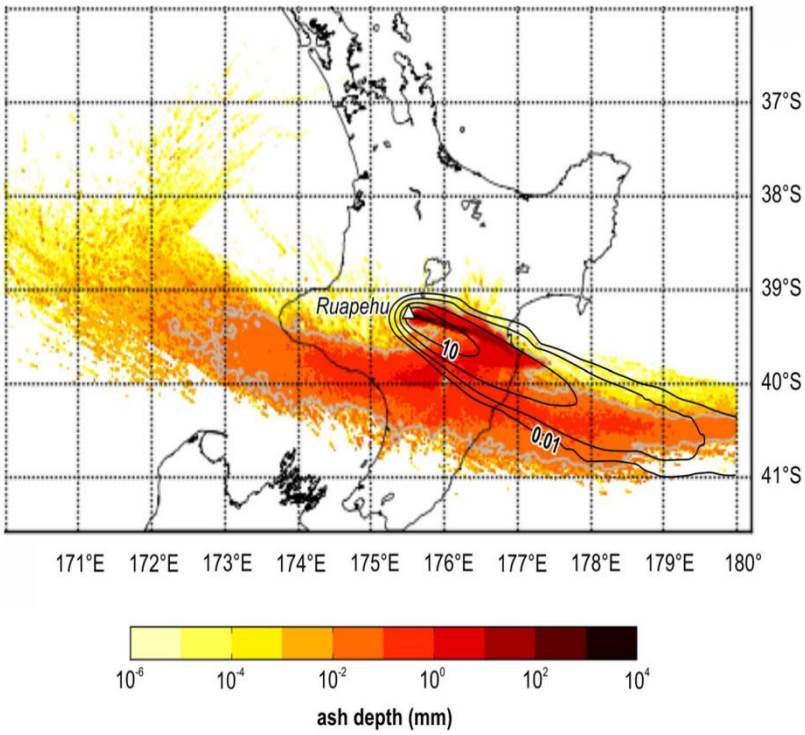

Fig. 17. Example of ash distribution forecast using HYSPLIT (Hurst and Davis, 2017)

The model calculation method of HYSPLIT is a hybrid between the Lagrangian approach, using a moving frame of reference for the advection and diffusion calculations as the trajectories or air parcels move from their initial location, and the Eulerian methodology, which uses a fixed three-dimensional grid as a frame of reference to compute pollutant air concentrations.

HYSPLIT simulation works for volcanic ash dispersion modeling as following conditions:

- Eruption input
- Meteorological data input

- Ash particle distribution
- Ash cloud
- Reduced ash
- Model output

All HYSPLIT options are available generally in the Windows-based version. HYSPLIT modeling system features :

A) Trajectories
- Single or multiple (space or time) simultaneous trajectories
- Optional grid of initial starting locations
- Computations forward or backward in time
- Default vertical motion using omega field
- Other motion options: isentropic, isosigma, isobaric, isopycnic
- Trajectory ensemble option using meteorological variations
- Output of meteorological variables along a trajectory
- Integrated trajectory clustering option

B) Air Concentrations

- 3D particle dispersion or splitting puffs (top-hat or Gaussian)
- Instantaneous or continuous emissions, point or area sources
- Multiple resolution concentration output grids
- Fixed concentration grid or dynamic sampling
- Wet and dry deposition, radioactive decay, and re-suspension
- Emission of multiple simultaneous pollutant species
- Automated source-receptor matrix computation
- Ensemble dispersion based on variations in meteorology, turbulence, or physics
- Concentration probability output for multiple simulations
- Integrated dust-storm emission algorithm
- Define rate constants to convert one species to another
- Mass can be transferred to a Eulerian module for global-scale simulations

C) Meteorology

- Model can run with multiple nested input data grids
- Links to ARL and NWS meteorological data server
- Utility programs to display and manipulate meteorological data

3.4.1 NOAA Satellite

HYSPLIT models acquire to simulate the dispersion and trajectory of substances transported and dispersed through our atmosphere, over local to global scales. National Oceanic and Atmospheric Administration (NOAA) is an American scientific and regulatory agency within the United States Department of Commerce that forecasts weather, monitors oceanic and atmospheric conditions. Meteorologists at the VAAC and the Meteorological Watch Offices use the HYSPLIT forecasts, among other sources of information, for writing Volcanic Ash Advisories and Significant Meteorological Information warning messages (called SIGMETs), respectively. The HYSPLIT dispersion forecasts are issued to the public and made available online in the website.

4. MATERIAL AND METHODS FOR SIMULATION

4.1 MATERIAL USED

The laptop device used in this thesis to develop the simulation results from HYSPLIT modelling system. Laptop is configured with the processor of 11th Gen Intel(R) Core(TM) i7-1165G7 and installed RAM of 16 GB. Laptop works with 64-bit Windows Operating System.

4.2 METHOD FOR SIMULATION

The simulation results obtained from HYSPLIT by NOAA. The simulation tests have been obtained from NOAA website. Other simulation details regarding the work function of HYSPLIT modelling system gathered from Hurst et al. (2017), INGV-CT, Webley et al. (2009) and documents from NOAA website.

5. RESULTS

5.1 MOUNT ETNA SIMULATIONS - OCTOBER 2021

In this section, Mount Etna volcanic region at different location from October 2021 have been simulated using HYSPLIT modelling system evolved by NOAA.

5.1.1 Test results of Volcanic ash particle concentration

In this section, the results were obtained for volcanic ash particle concentration at mg/m^2 which have been evaluated using HYSPLIT modeling system from October 2021 data. The Mount Etna located at 37.734^0 N 15.004^0 E, where the mass concentration evaluated in given in Fig. 18. The data set comprises of October month.

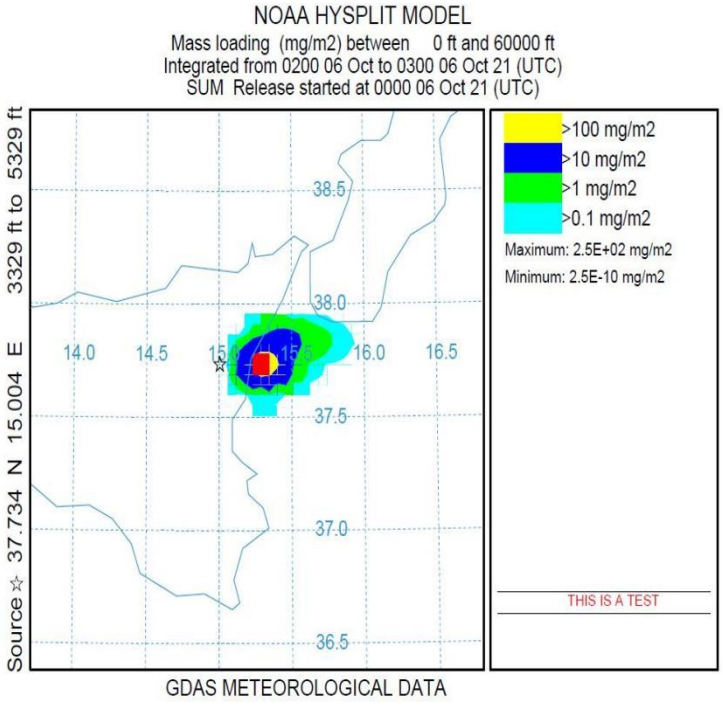

Fig. 18. Volcanic ash concentration (mg/m^2) at Mount Etna (37.734^0 N 15.004^0 E) using HYSPLIT modeling system

Another location from Mount Etna (37.752^0 N 14.995^0 E) where the ash particle mass concentration have been evaluated at mg/m^2. The measurements were taken in three parts for the data set in this particular location.

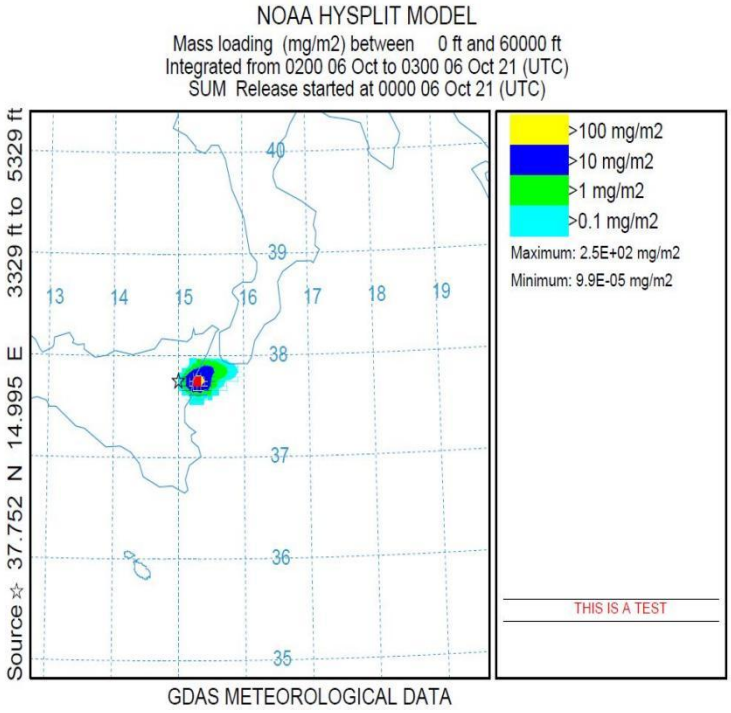

Fig. 19. Volcanic ash concentration (mg/m^2) at Mount Etna (37.752^0 N 14.995^0 E) using HYSPLIT modeling system

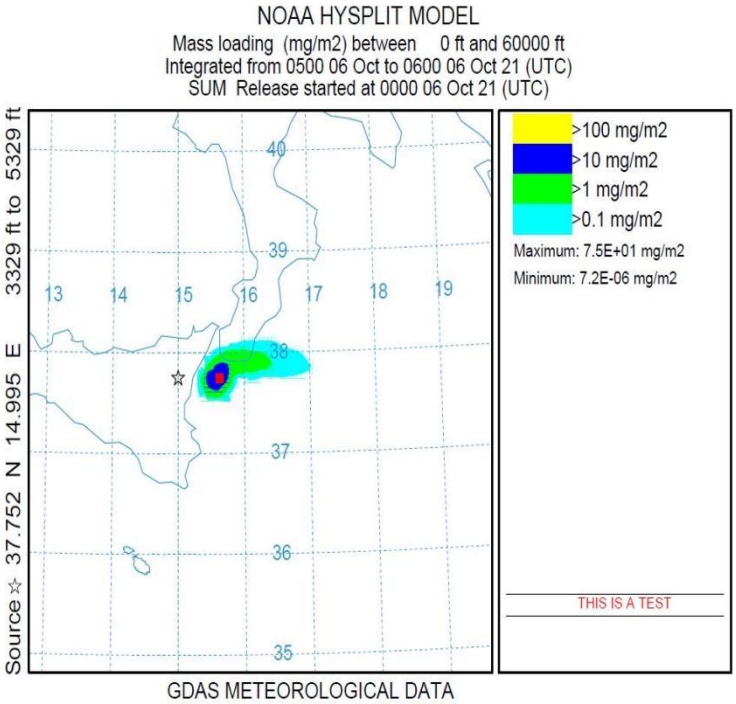

Fig. 20. Volcanic ash concentration (mg/m^2) at Mount Etna (37.752^0 N 14.995^0 E) using HYSPLIT modeling system

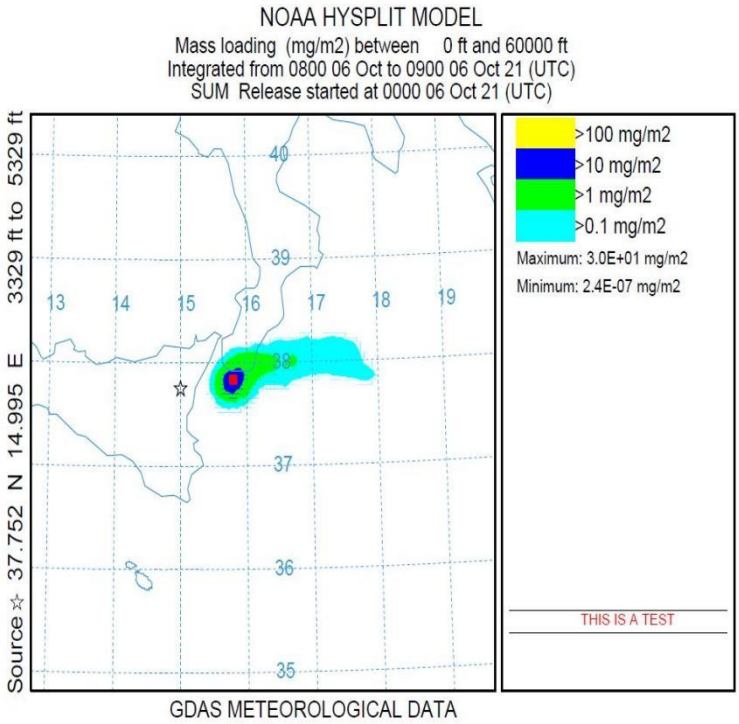

Fig. 21. Volcanic ash concentration (mg/m^2) at Mount Etna (37.752^0 N 14.995^0 E) using HYSPLIT modeling system

Other location of Mount Etna, 37.752^0 N 14.991^0 E from the measurement for volcanic ash concentration at mg/m^2

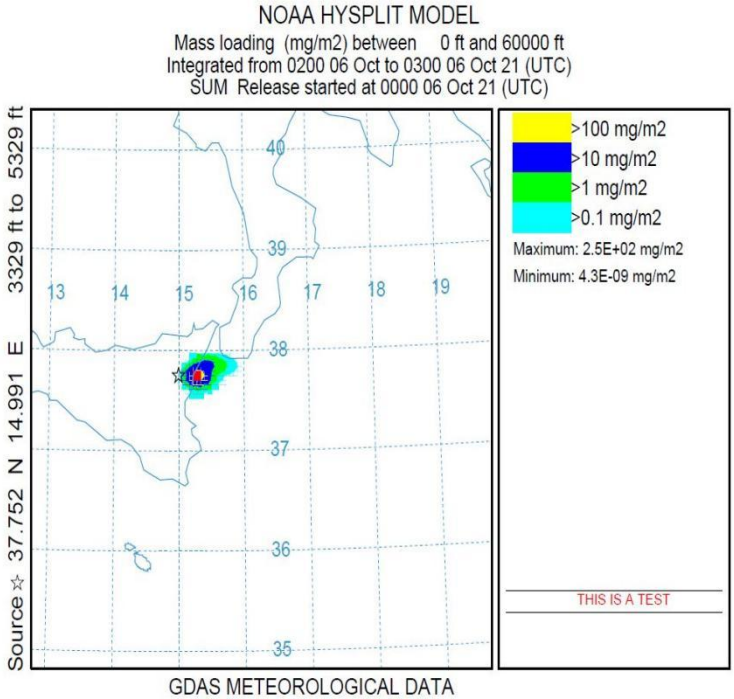

Fig. 22. Volcanic ash concentration (mg/m^2) at Mount Etna (37.752^0 N 14.991^0 E) using HYSPLIT modeling system

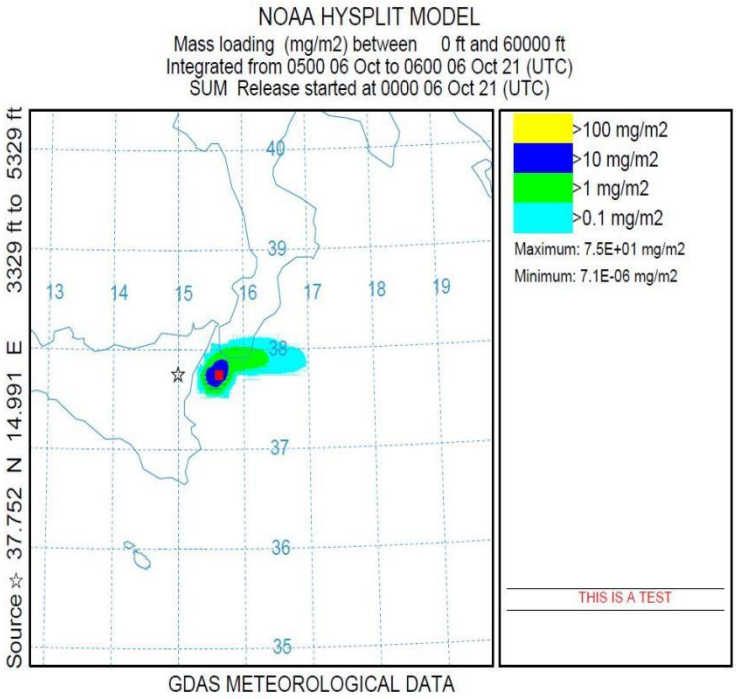

Fig. 23. Volcanic ash concentration (mg/m^2) at Mount Etna (37.752^0 N 14.991^0 E) using HYSPLIT modeling system

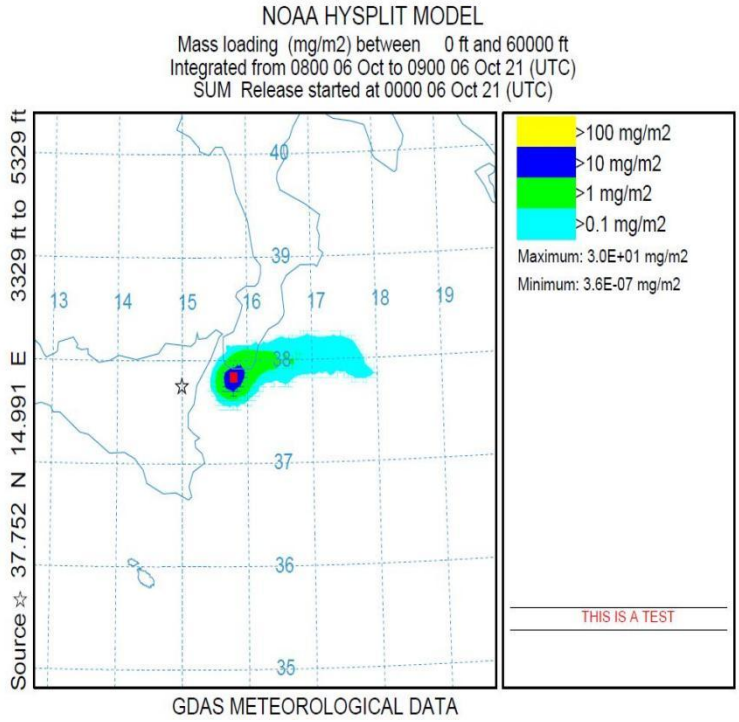

Fig. 24. Volcanic ash concentration (mg/m^2) at Mount Etna (37.752^0 N 14.991^0 E) using HYSPLIT modeling system

Other measurement for ash concentration at mg/m^2 comprises the summit location of Mount Etna (37.751^0 N 14.993^0 E)

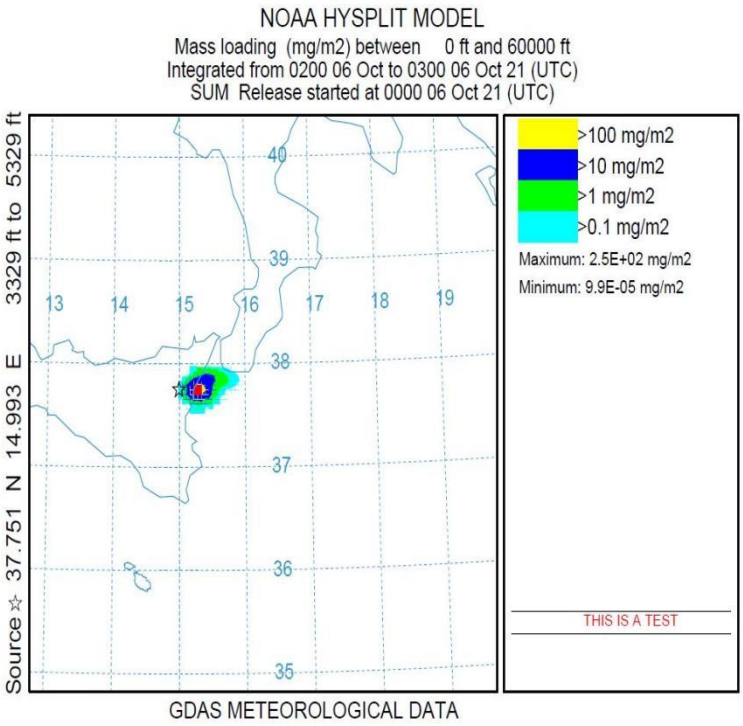

Fig. 25. Volcanic ash concentration (mg/m^2) at Mount Etna (37.751^0 N 14.993^0 E) using HYSPLIT modeling system

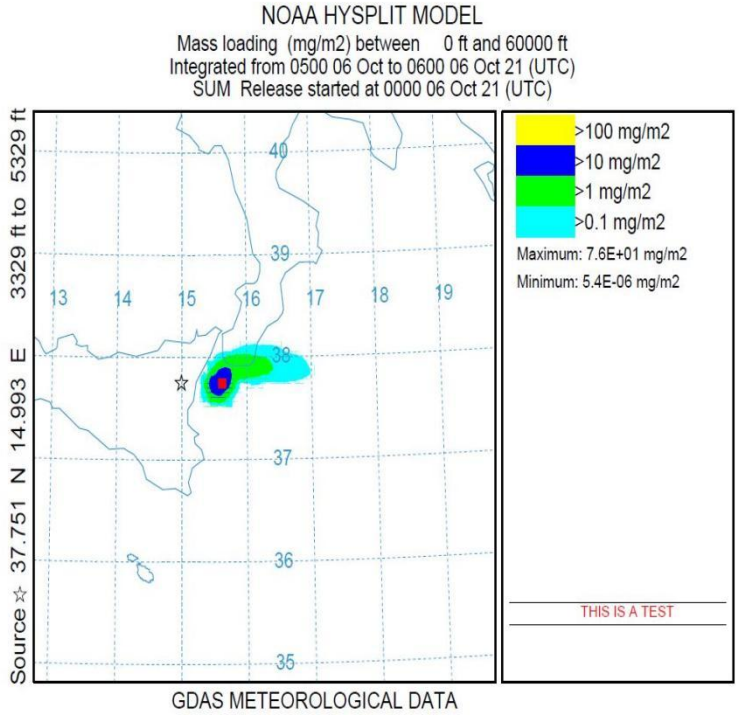

Fig. 26. Volcanic ash concentration (mg/m^2) at Mount Etna (37.751^0 N 14.993^0 E) using HYSPLIT modeling system

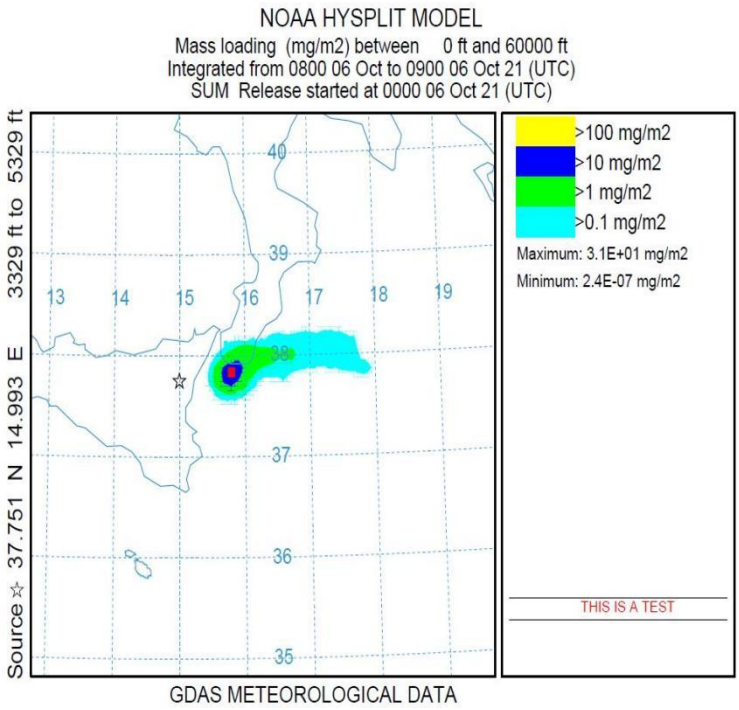

Fig. 27. Volcanic ash concentration (mg/m^2) at Mount Etna (37.751^0 N 14.993^0 E) using HYSPLIT modeling system

5.1.2 Test results of ash particle position

The ash particle positions from Mount Etna at different locations have been simulated using HYSPLIT modelling system by NOAA. In Fig. 28 ash particle positions simulated from Mount Etna (37.734^0 N 15.004^0 E) location.

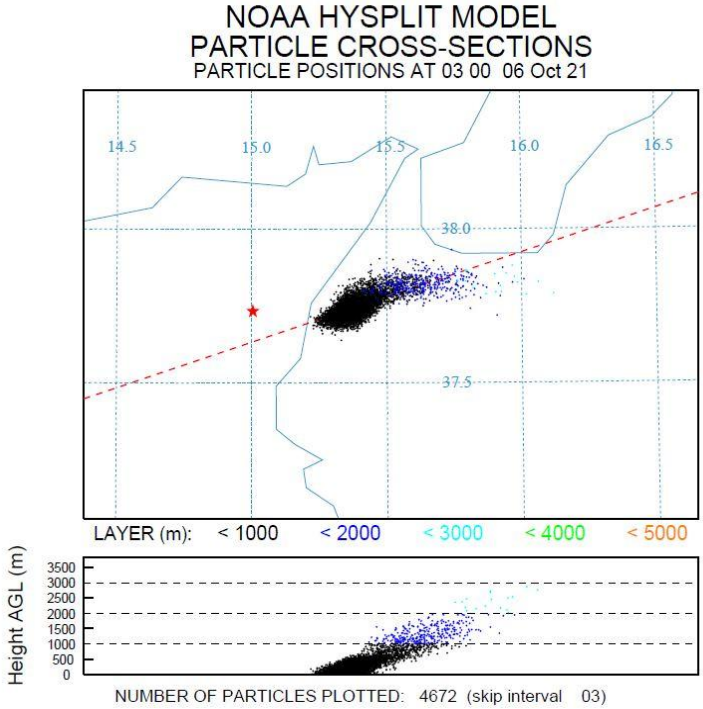

Fig. 28. ash particle positions in ABL at Mount Etna (37.734^0 N 15.004^0 E) using HYSPLIT modeling system

Second location from Mount Etna (37.752^0 N 14.995^0 E) have been taken for ash particle positions in ABL. The ash particle positions have been simulated using HYSPLIT by NOAA.

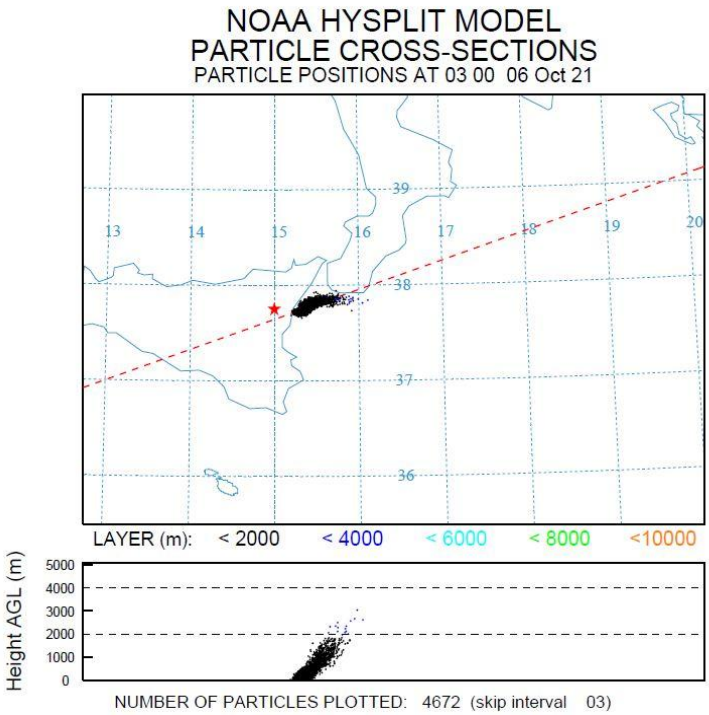

Fig. 29. ash particle positions in ABL at Mount Etna (37.752^0 N 14.995^0 E) using HYSPLIT modeling system

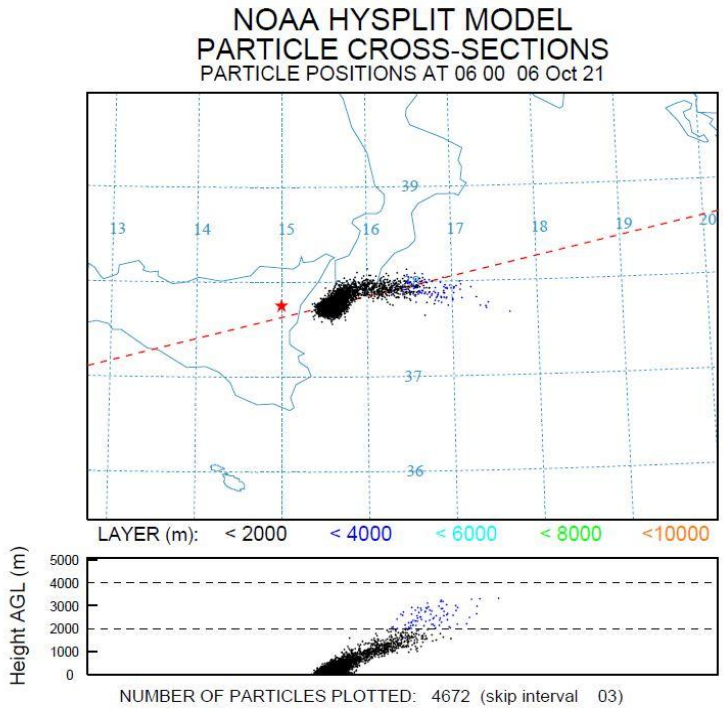

Fig. 30. ash particle positions in ABL at Mount Etna (37.752^0 N 14.995^0 E) using HYSPLIT modeling system

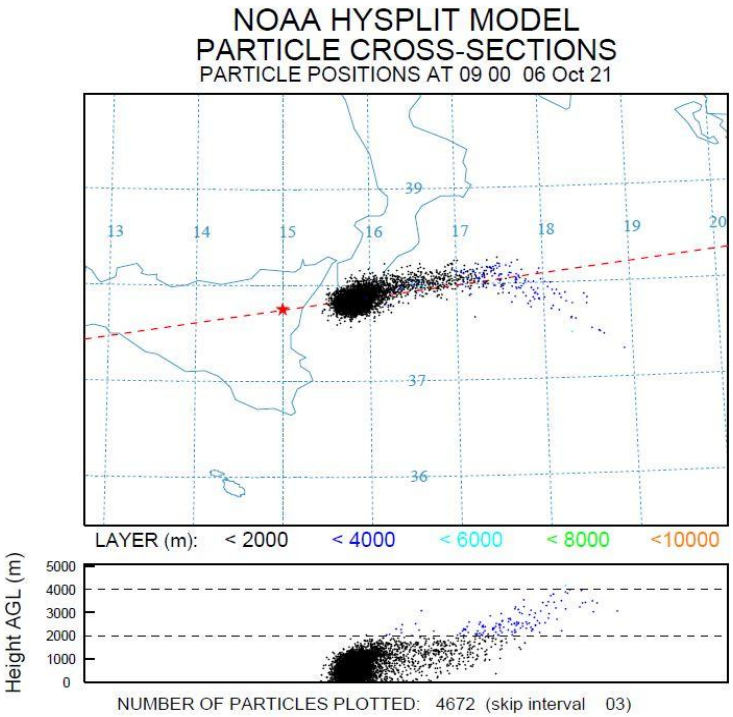

Fig. 31. ash particle positions in ABL at Mount Etna (37.752^0 N 14.995^0 E) using HYSPLIT modeling system

Another location from Mount Etna (37.752^0 N 14.991^0 E) taken simulations for ash particle concentrations in ABL. Simulations done using HYSPLIT modelling system evolved by NOAA.

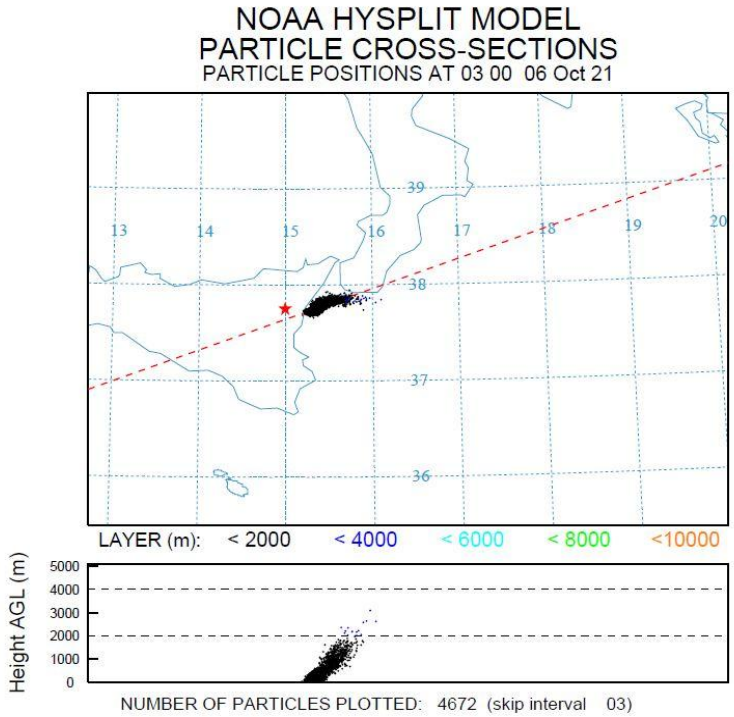

Fig. 32. ash particle positions in ABL at Mount Etna (37.752^0 N 14.991^0 E) using HYSPLIT modeling system

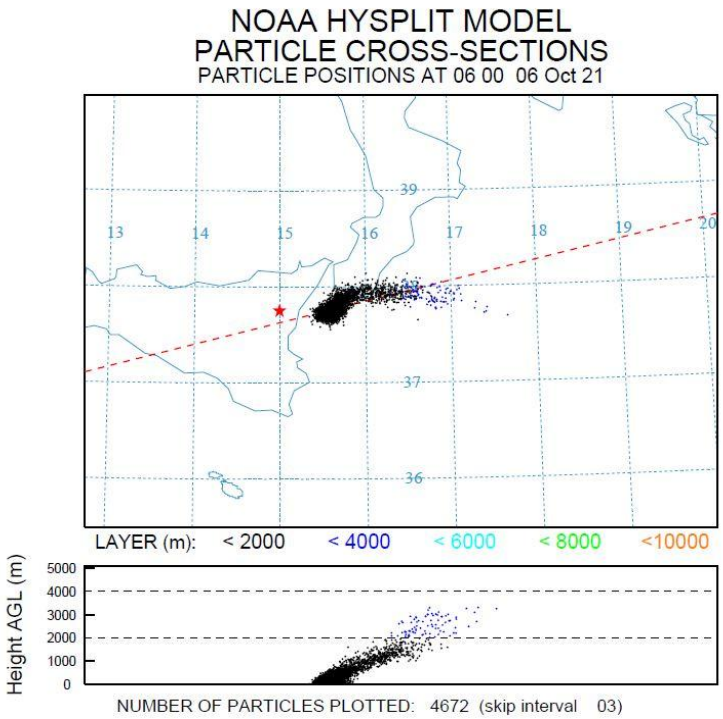

Fig. 33. ash particle positions in ABL at Mount Etna (37.752^0 N 14.991^0 E) using HYSPLIT modeling system

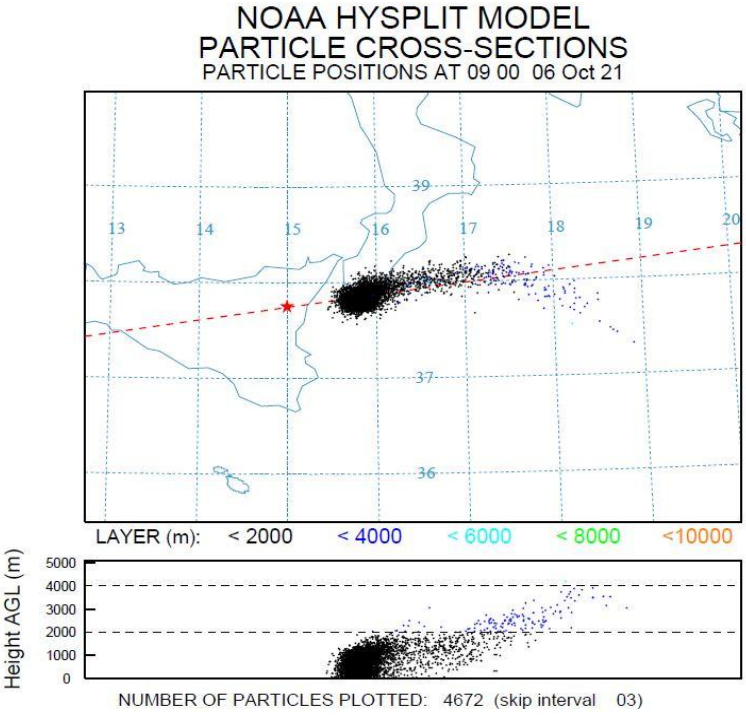

Fig. 34. ash particle positions in ABL at Mount Etna (37.752^0 N 14.991^0 E) using HYSPLIT modeling system

One more location from the volcanic region of Mount Etna has been taken at 37.751^0 N 14.993^0 E.

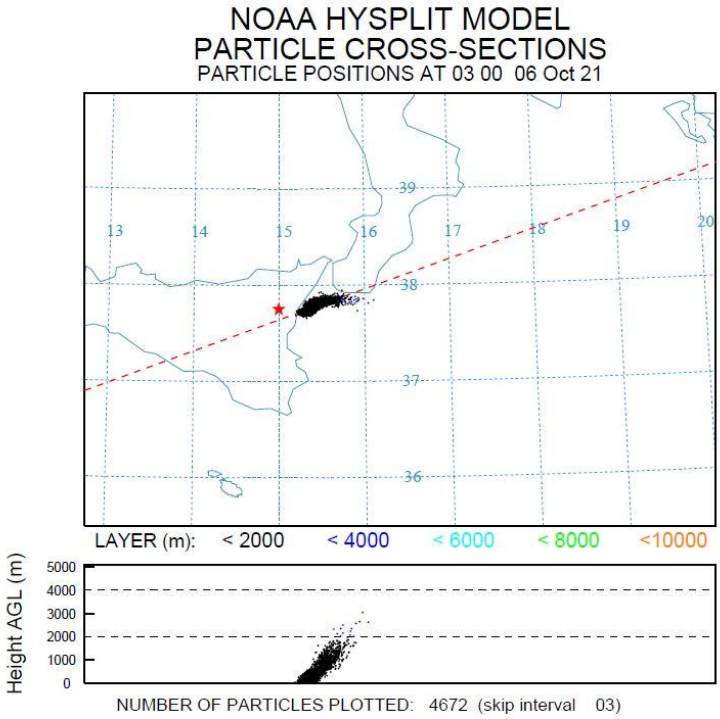

Fig. 35. ash particle positions in ABL at Mount Etna (37.751^0 N 14.993^0 E) using HYSPLIT modeling system

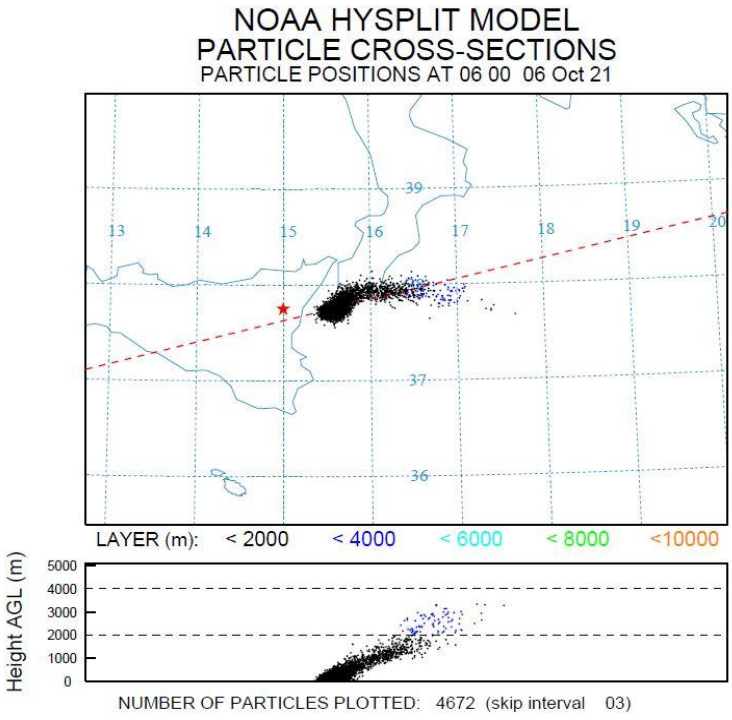

Fig. 36. ash particle positions in ABL at Mount Etna (37.751^0 N 14.993^0 E) using HYSPLIT modeling system

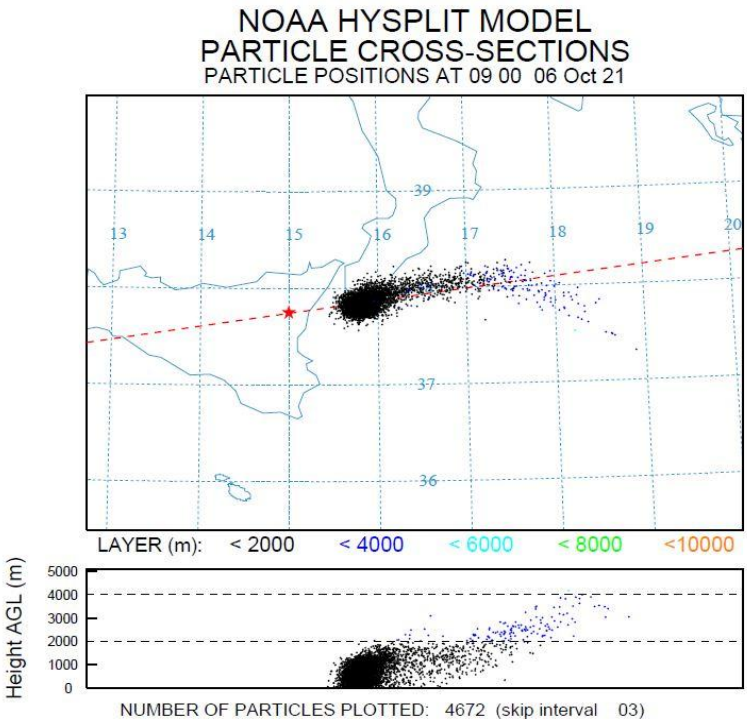

Fig. 37. ash particle positions in ABL at Mount Etna (37.751^0 N 14.993^0 E) using HYSPLIT modeling system

5.2 MOUNT ETNA ERUPTION MONTH (FEBRUARY 2021)

5.2.1 Volcanic ash particle position

This section obtains simulation results from February 2021 month data. Starting with 1st Feb. 2021 ash particle position of Mount Etna volcano.

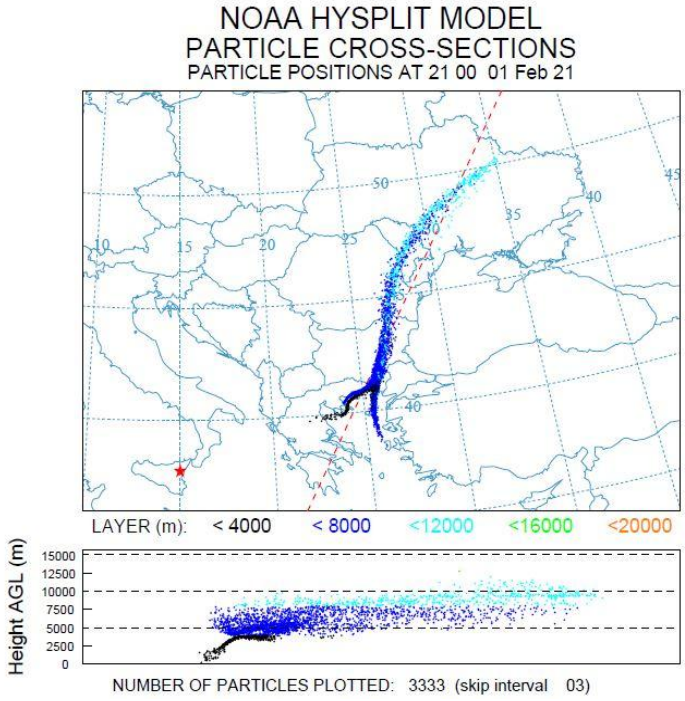

Fig. 38. ash particle positions in ABL at Mount Etna (1st Feb. 2021) using HYSPLIT modeling system

8th Feb. 2021

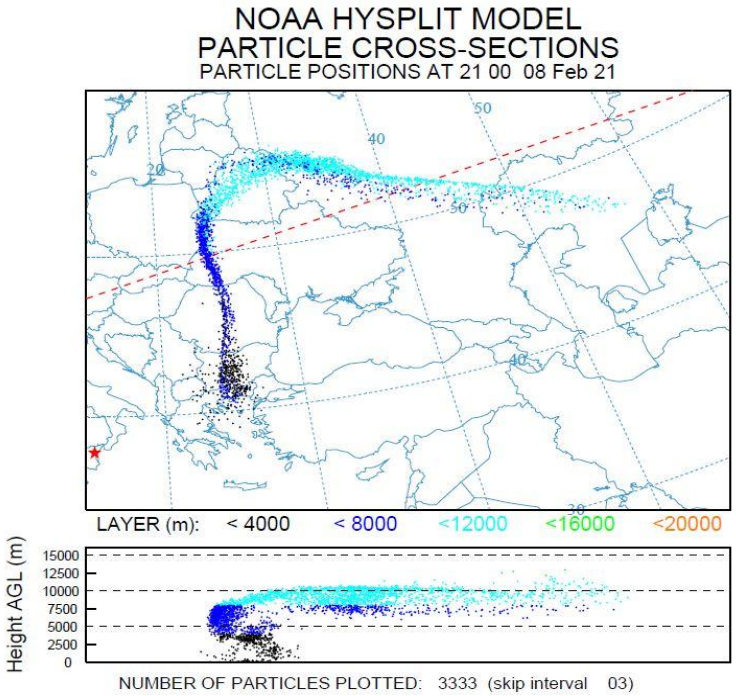

Fig. 39. ash particle positions in ABL at Mount Etna (8th Feb. 2021) using HYSPLIT modeling system

10th Feb. 2021

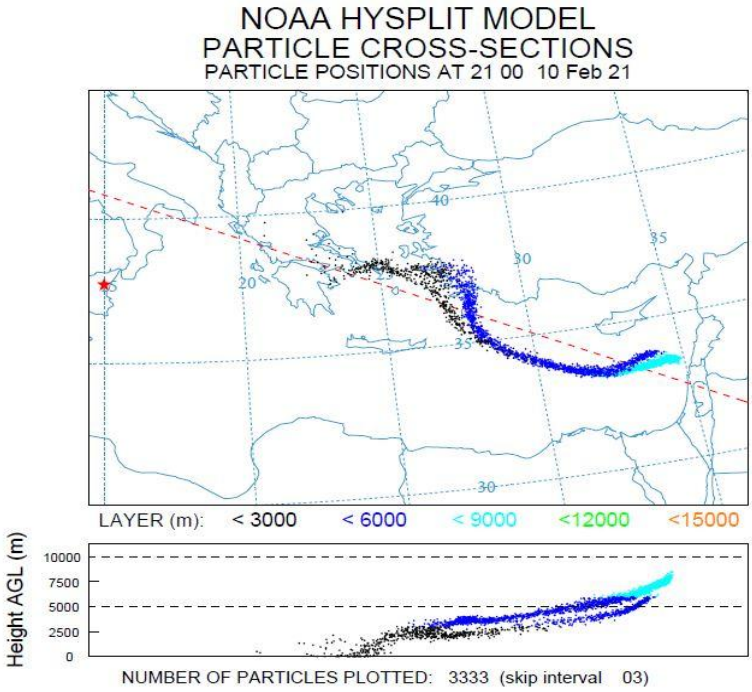

Fig. 40. ash particle positions in ABL at Mount Etna (10th Feb.) using HYSPLIT modeling system

11th Feb. 2021

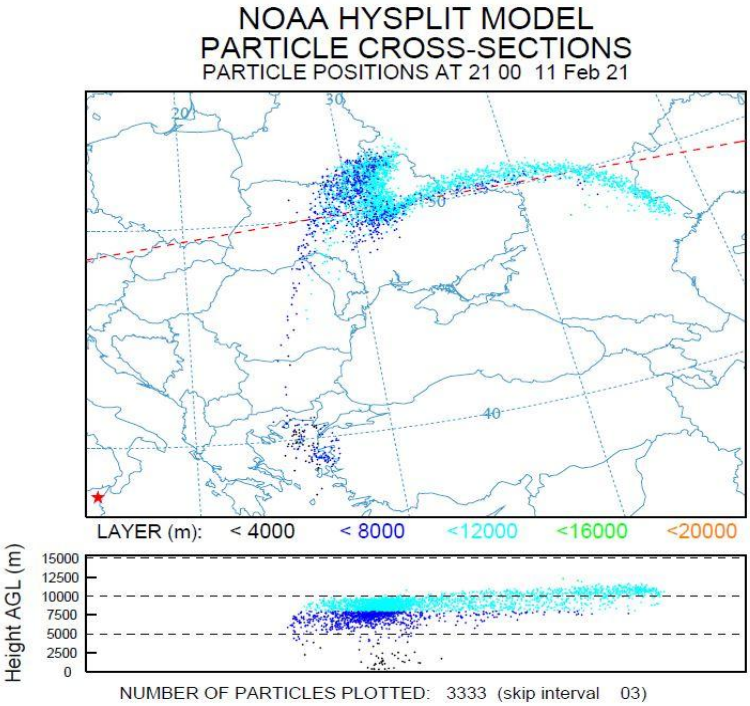

Fig. 41. ash particle positions in ABL at Mount Etna (11th Feb. 2021) using HYSPLIT modeling system

12th Feb. 2021

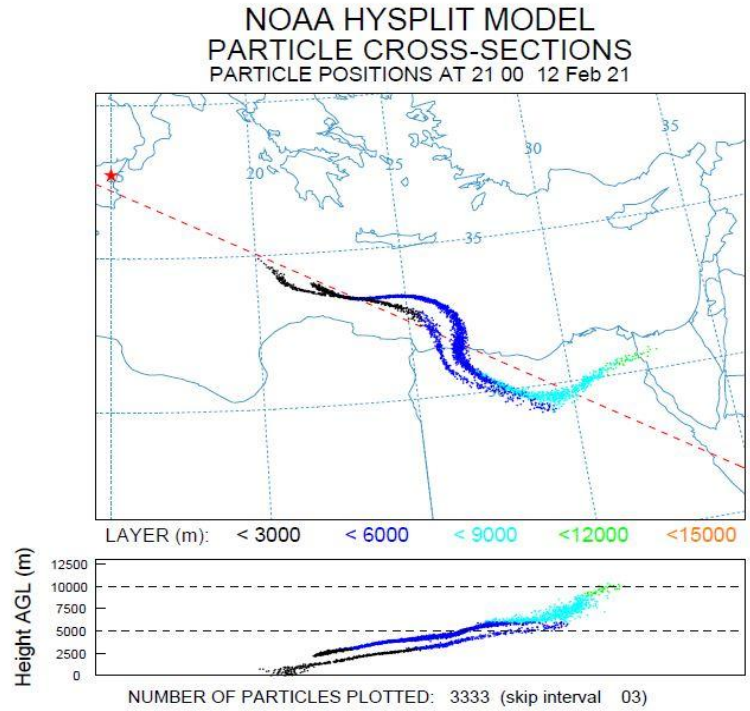

Fig. 42. ash particle positions in ABL at Mount Etna (12th Feb. 2021) using HYSPLIT modeling system

15th Feb. 2021

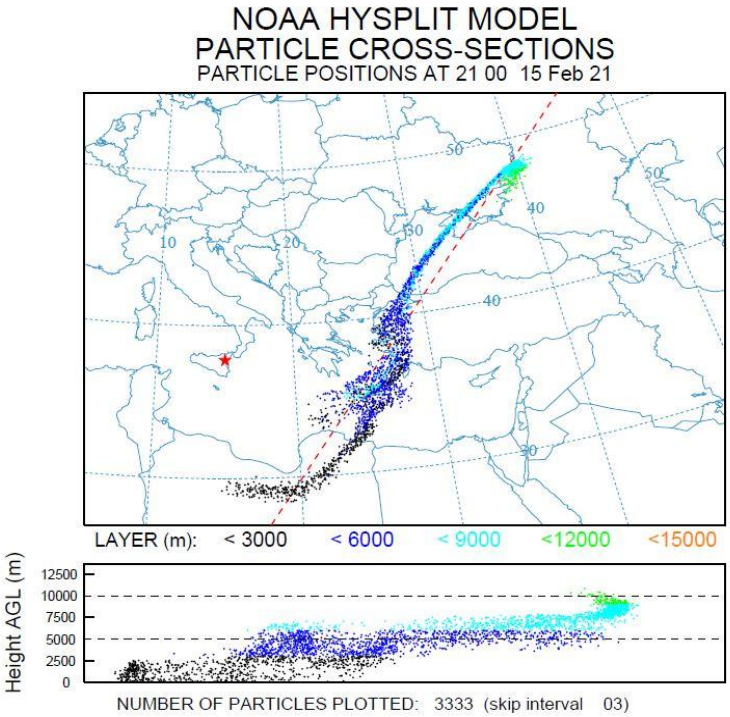

Fig. 43. ash particle positions in ABL at Mount Etna (15th Feb. 2021) using HYSPLIT modeling system

16th Feb. 2021 (Eruption day)

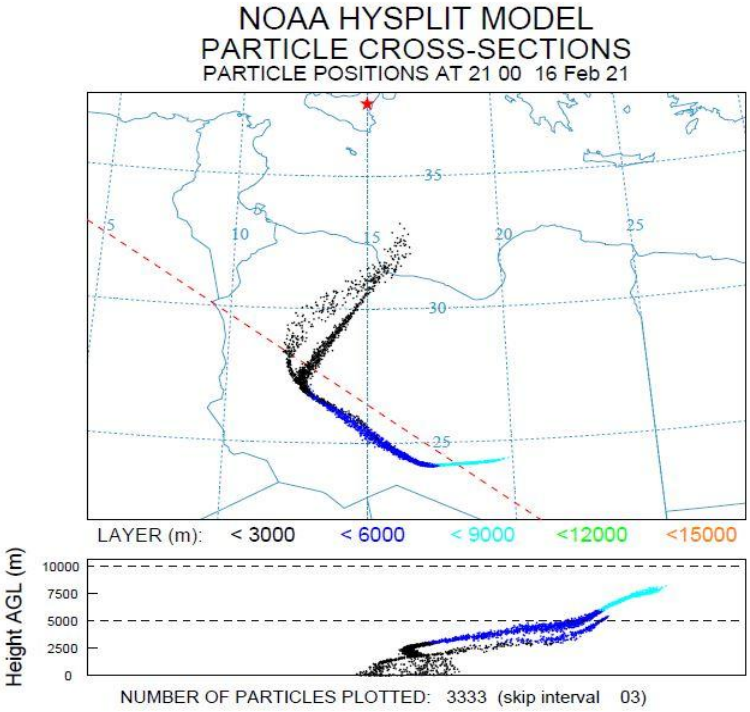

Fig. 44. ash particle positions in ABL at Mount Etna (16th Feb. 2021) using HYSPLIT modeling system

17th Feb. 2021 (later day after eruption)

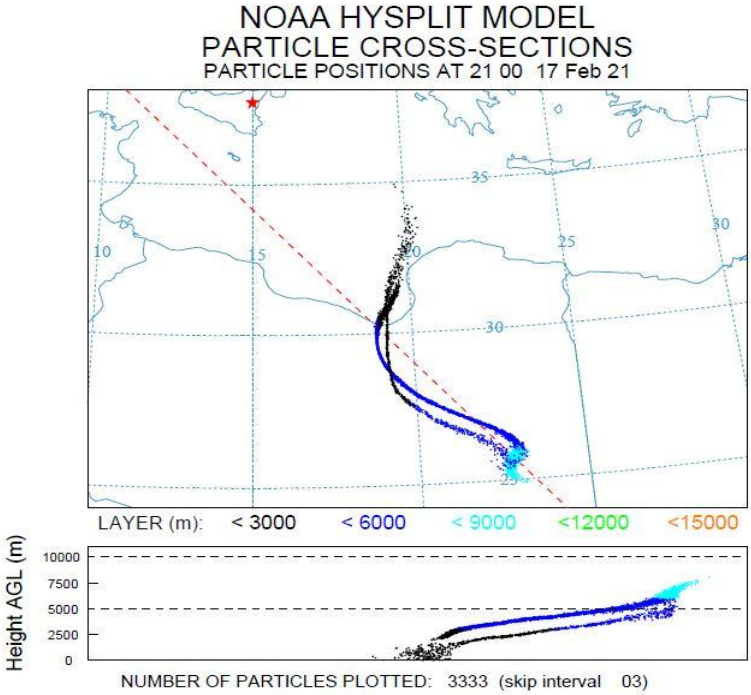

Fig. 45. ash particle positions in ABL at Mount Etna (17th Feb. 2021) using HYSPLIT modeling system

18th Feb. 2021

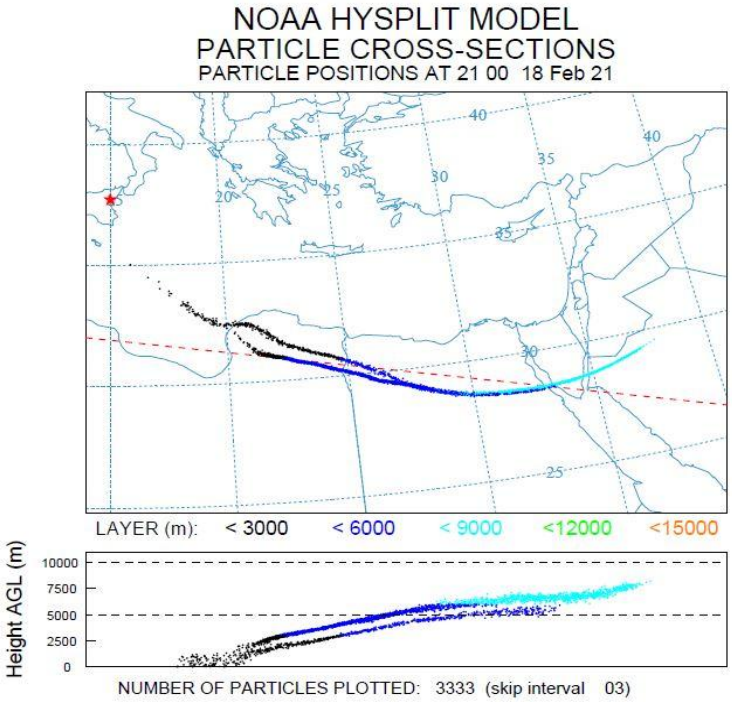

Fig. 46. ash particle positions in ABL at Mount Etna (18th Feb. 2021) using HYSPLIT modeling system

22nd Feb. 2021

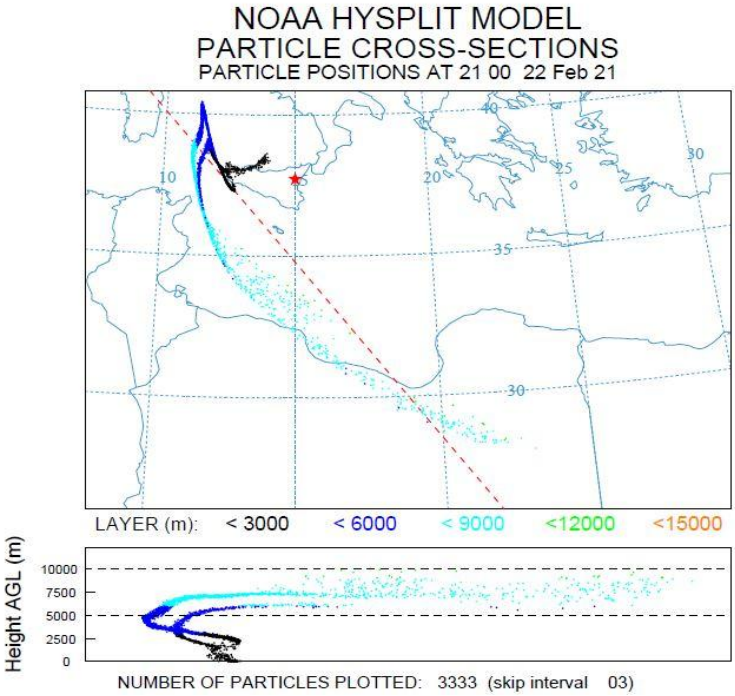

Fig. 47. ash particle positions in ABL at Mount Etna (22nd Feb. 2021) using HYSPLIT modeling system

28th Feb. 2021

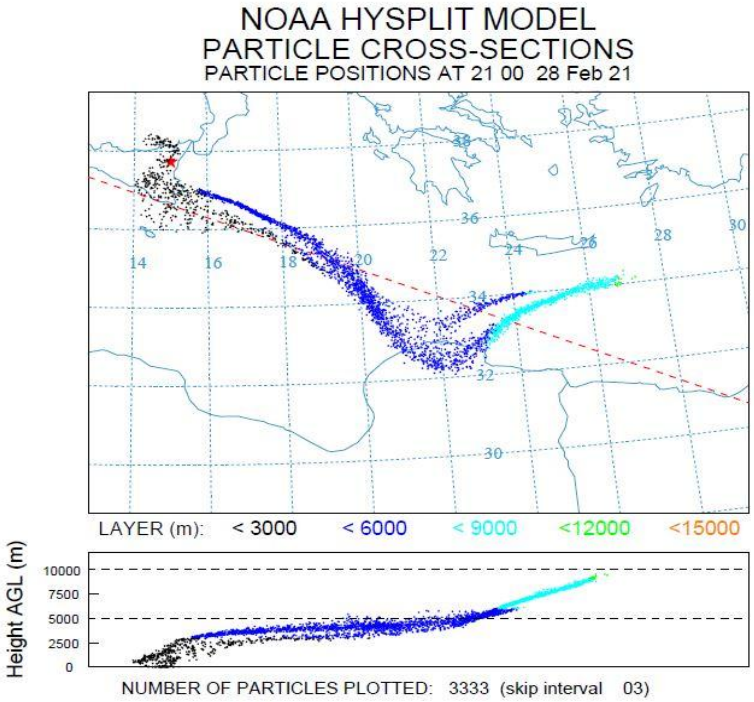

Fig. 48. ash particle positions in ABL at Mount Etna (28th Feb. 2021) using HYSPLIT modeling system

10th March 2021

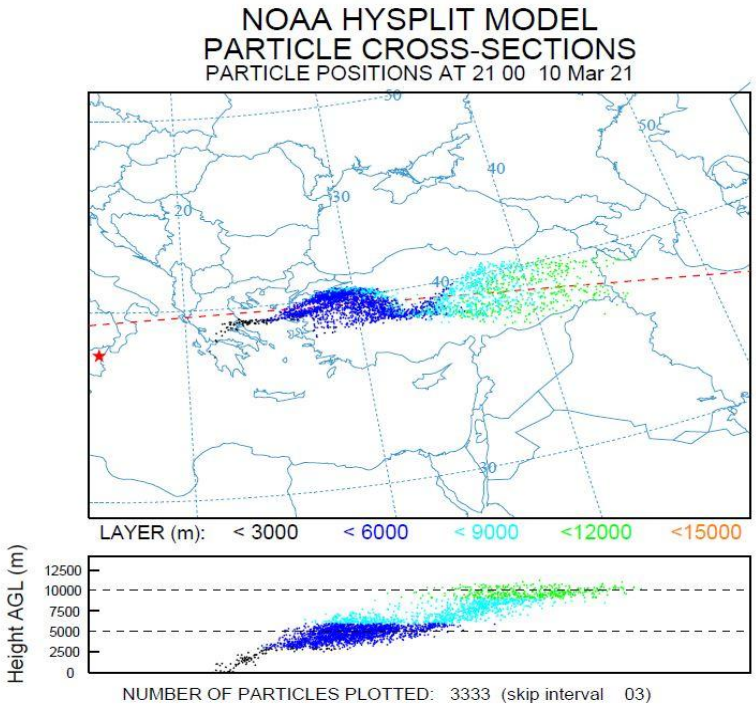

Fig. 49. ash particle positions in ABL at Mount Etna (10th March 2021) using HYSPLIT modeling system

16th March 2021

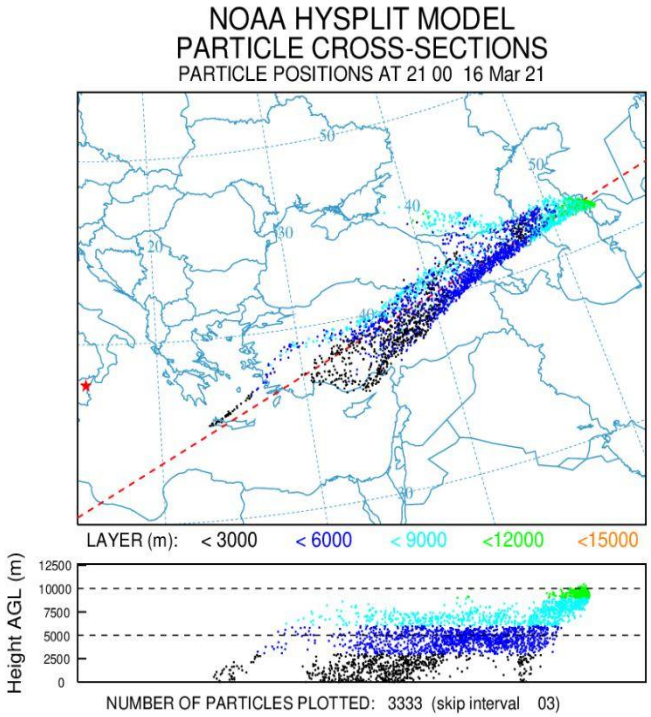

Fig. 50. ash particle positions in ABL at Mount Etna (16th March 2021) using HYSPLIT modeling system

5.2.2 Ash particle deposition

1st Feb. 2021

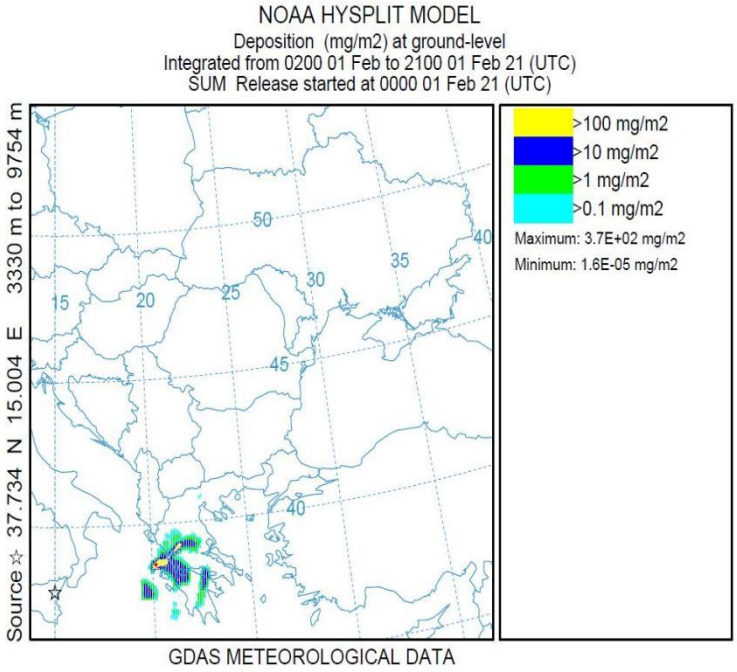

Fig. 51. ash particle deposition in ABL at Mount Etna (1st Feb. 2021) using HYSPLIT modeling system

8th Feb. 2021

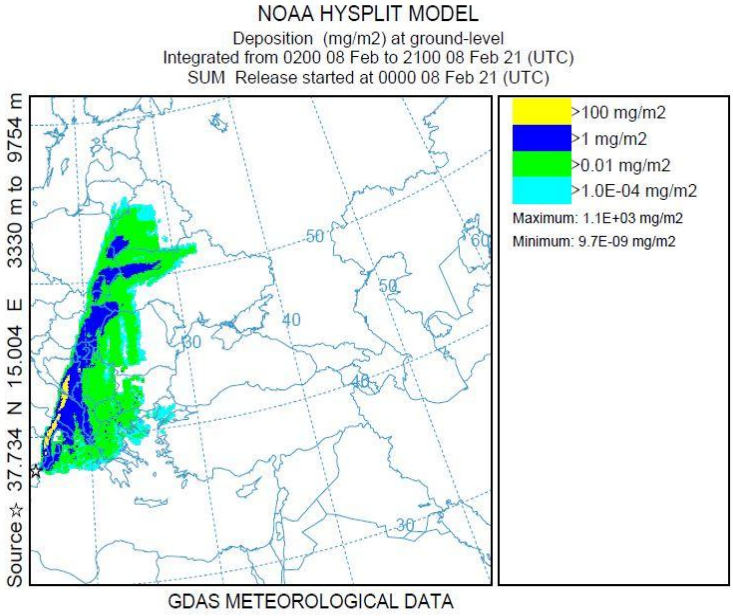

Fig. 52. ash particle deposition in ABL at Mount Etna (8th Feb. 2021) using HYSPLIT modeling system

10th Feb. 2021

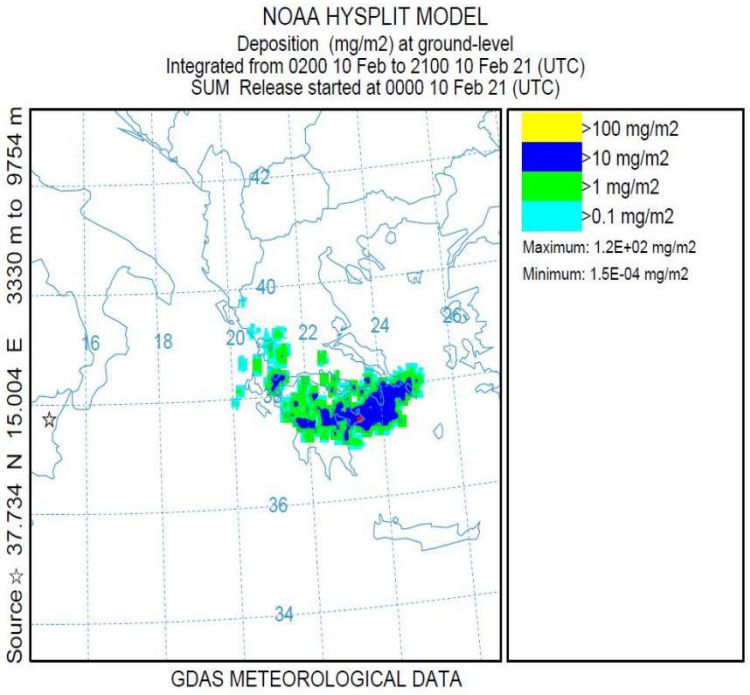

Fig. 53. ash particle deposition in ABL at Mount Etna (10th Feb. 2021) using HYSPLIT modeling system

11th Feb. 2021

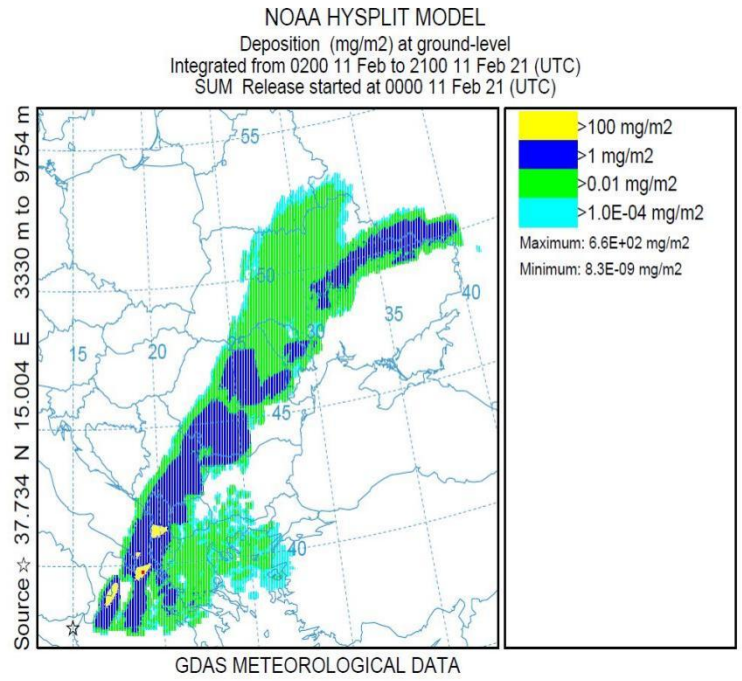

Fig. 54. ash particle deposition in ABL at Mount Etna (11th Feb. 2021) using HYSPLIT modeling system

12th Feb. 2021

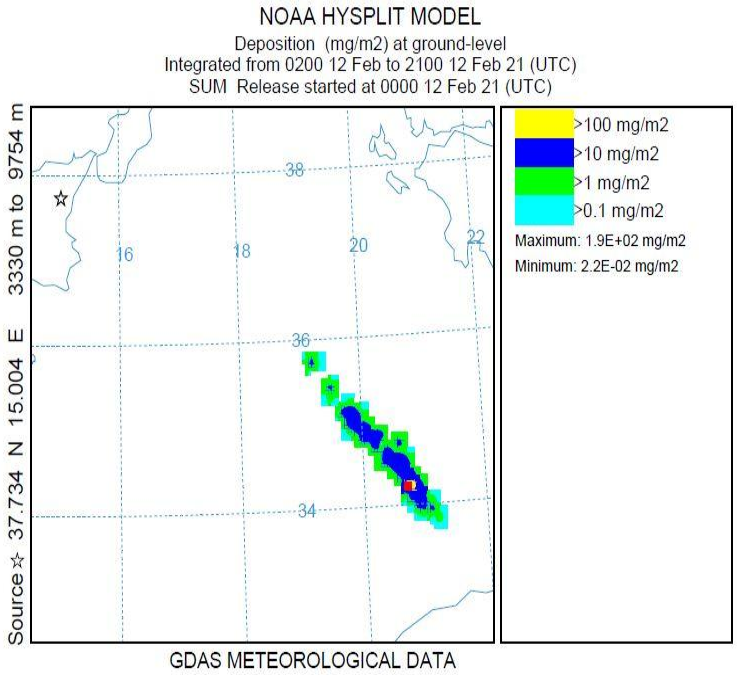

Fig. 55. ash particle deposition in ABL at Mount Etna (12th Feb. 2021) using HYSPLIT modeling system

15th Feb. 2021

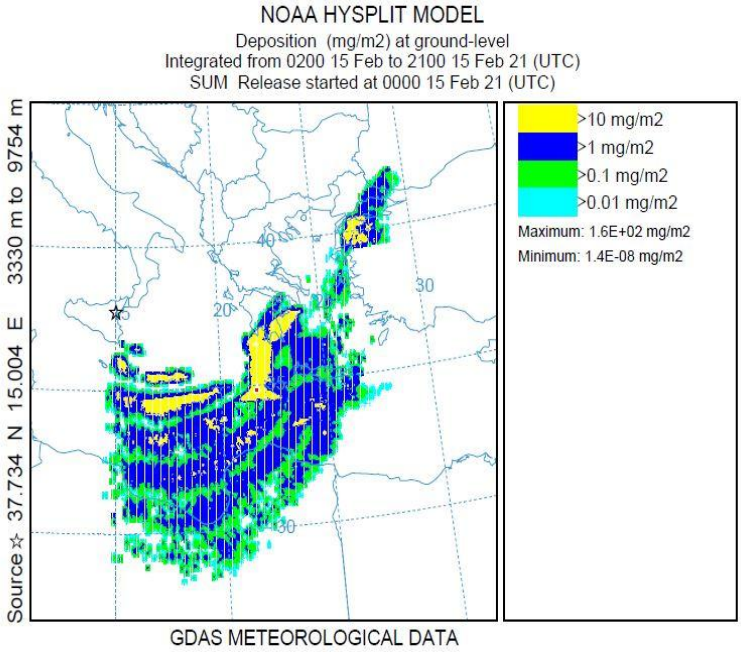

Fig. 56. ash particle deposition in ABL at Mount Etna (15th Feb. 2021) using HYSPLIT modeling system

16th Feb. 2021

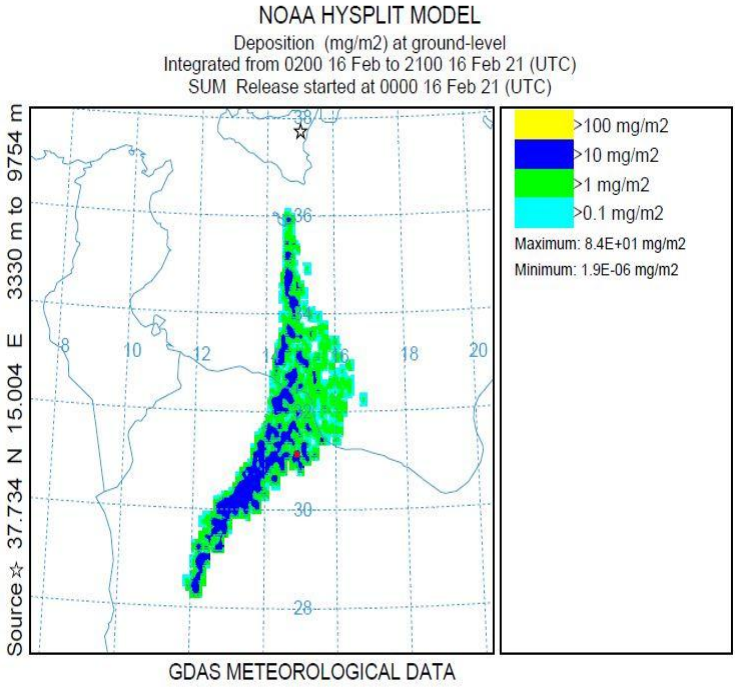

Fig. 57. ash particle deposition in ABL at Mount Etna (16th Feb. 2021) using HYSPLIT modeling system

17th Feb. 2021

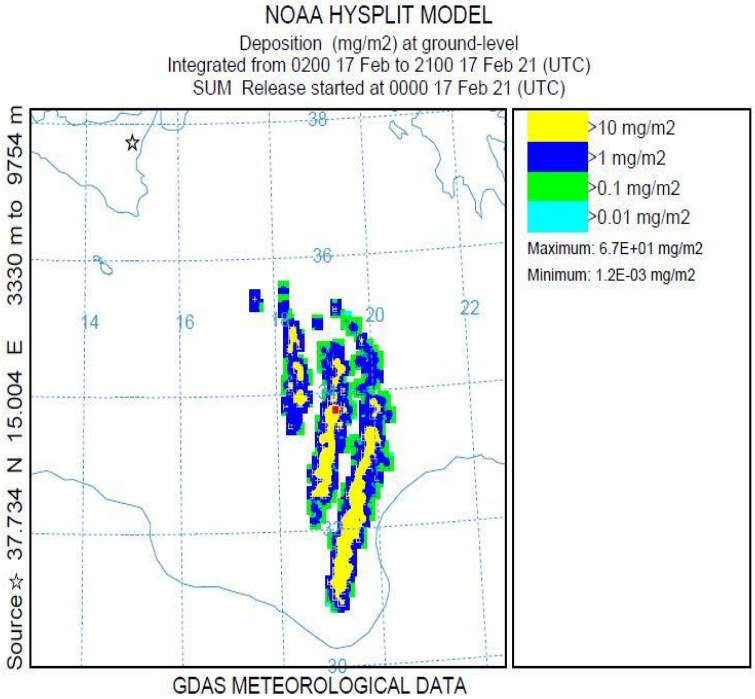

Fig. 58. ash particle deposition in ABL at Mount Etna (17th Feb. 2021) using HYSPLIT modeling system

18th Feb. 2021

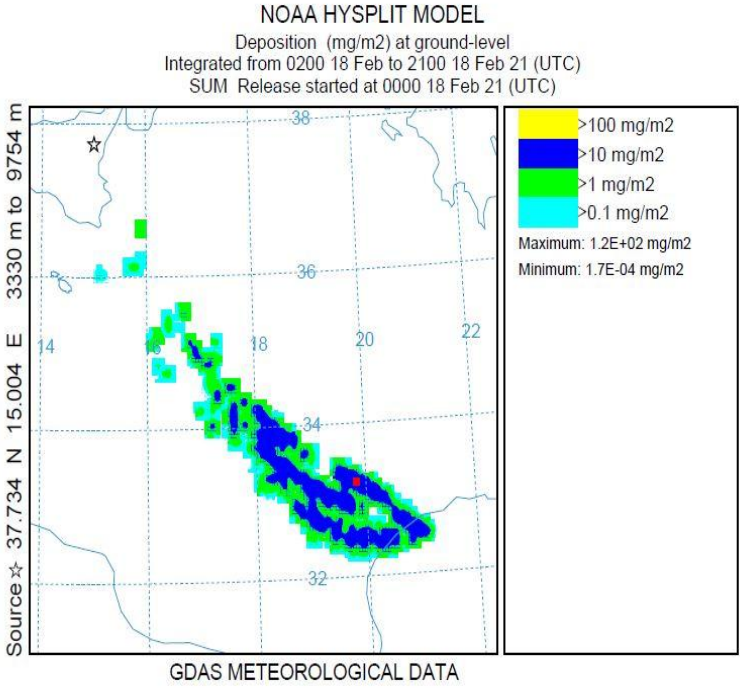

Fig. 59. ash particle deposition in ABL at Mount Etna (18th Feb. 2021) using HYSPLIT modeling system

22nd Feb. 2021

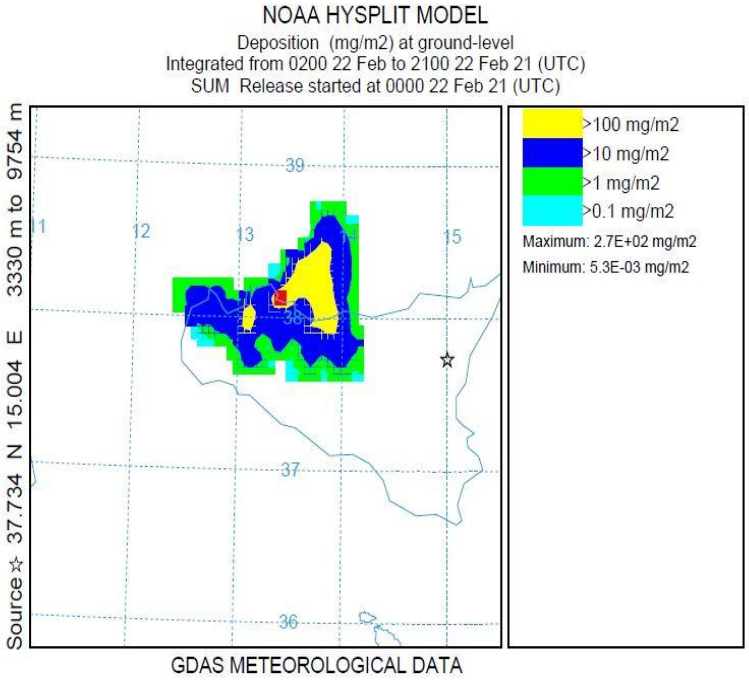

Fig. 60. ash particle deposition in ABL at Mount Etna (22nd Feb. 2021) using HYSPLIT modeling system

28th Feb. 2021

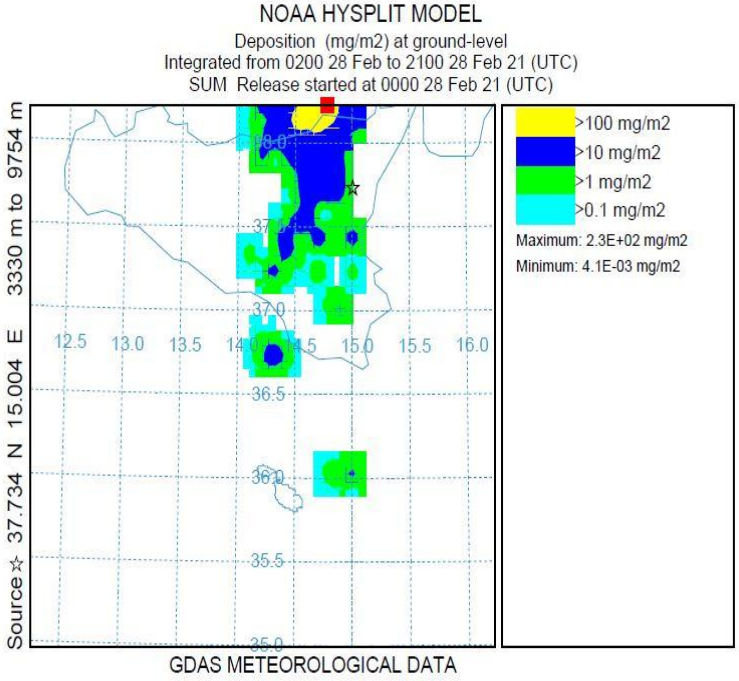

Fig. 61. ash particle deposition in ABL at Mount Etna (28th Feb. 2021) using HYSPLIT modeling system

10th March 2021

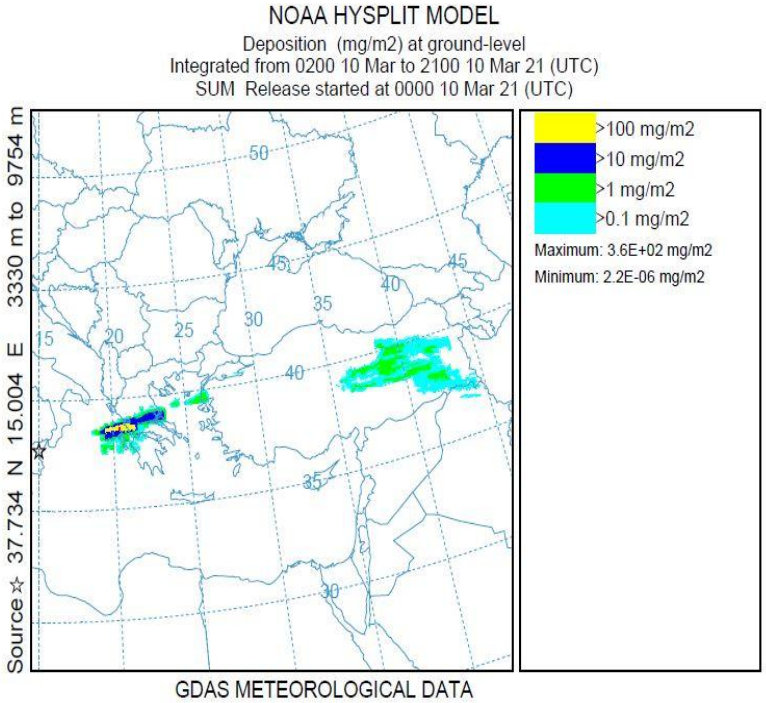

Fig. 62. ash particle deposition in ABL at Mount Etna (10th March 2021) using HYSPLIT modeling system

16th March 2021

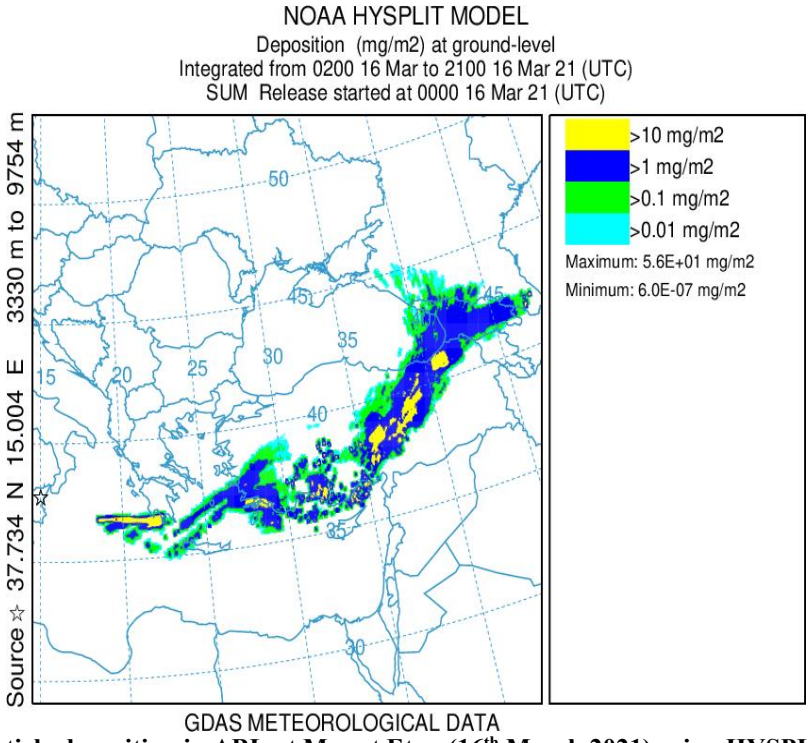

Fig. 63. ash particle deposition in ABL at Mount Etna (16th March 2021) using HYSPLIT modeling system

5.2.3 Ash particle concentration

1st Feb. 2021

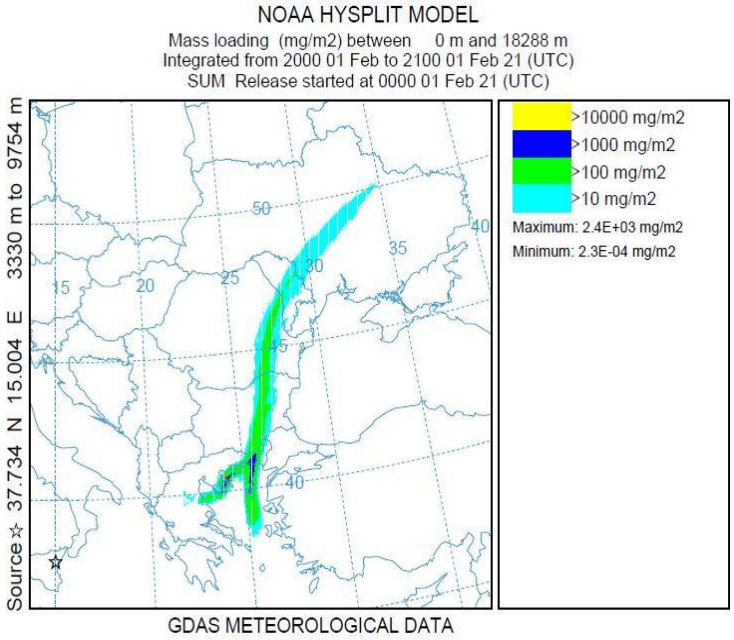

Fig. 64. ash particle concentration in ABL at Mount Etna (1st Feb. 2021) using HYSPLIT modeling system

8th Feb. 2021

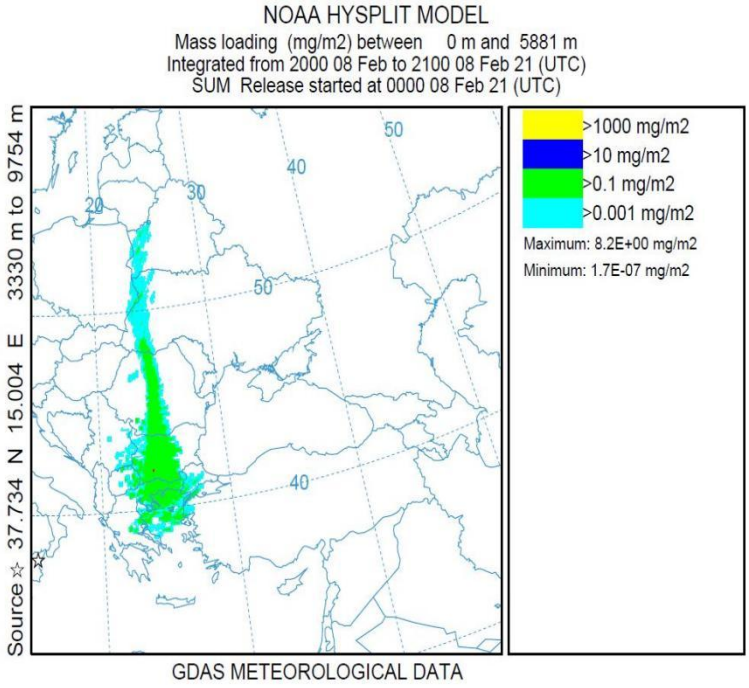

Fig. 65. ash particle concentration in ABL at Mount Etna (8th Feb. 2021) using HYSPLIT modeling system

10th Feb. 2021

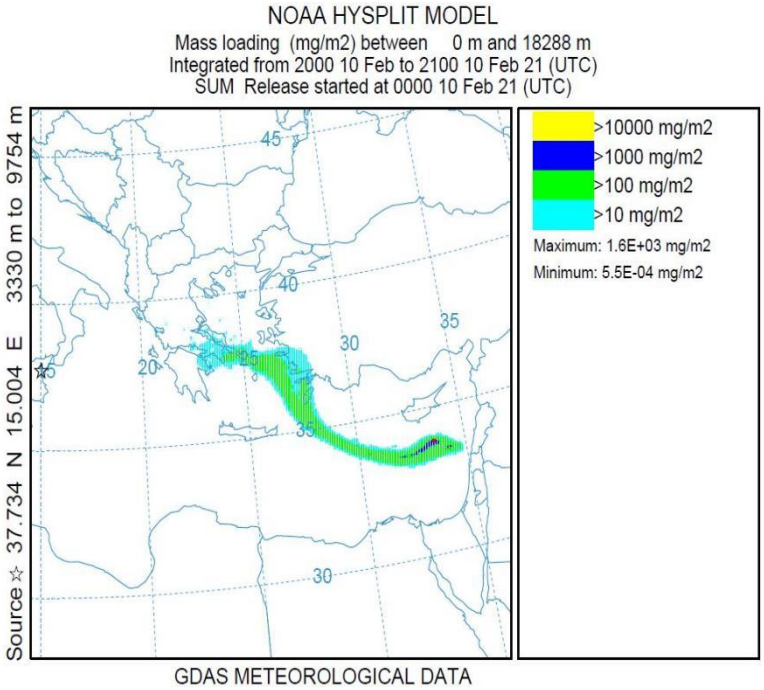

Fig. 66. ash particle concentration in ABL at Mount Etna (10th Feb. 2021) using HYSPLIT modeling system

11th Feb. 2021

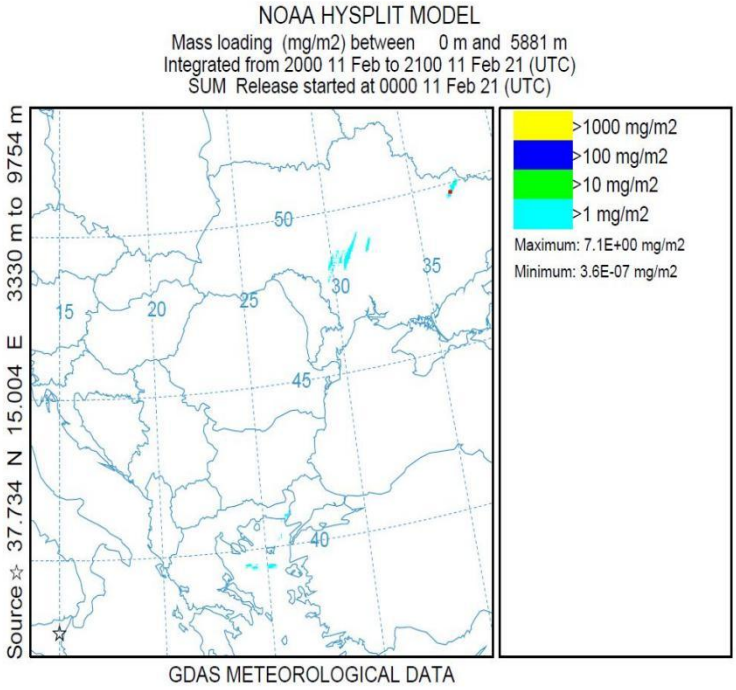

Fig. 67. ash particle concentration in ABL at Mount Etna (11th Feb. 2021) using HYSPLIT modeling system

12th Feb. 2021

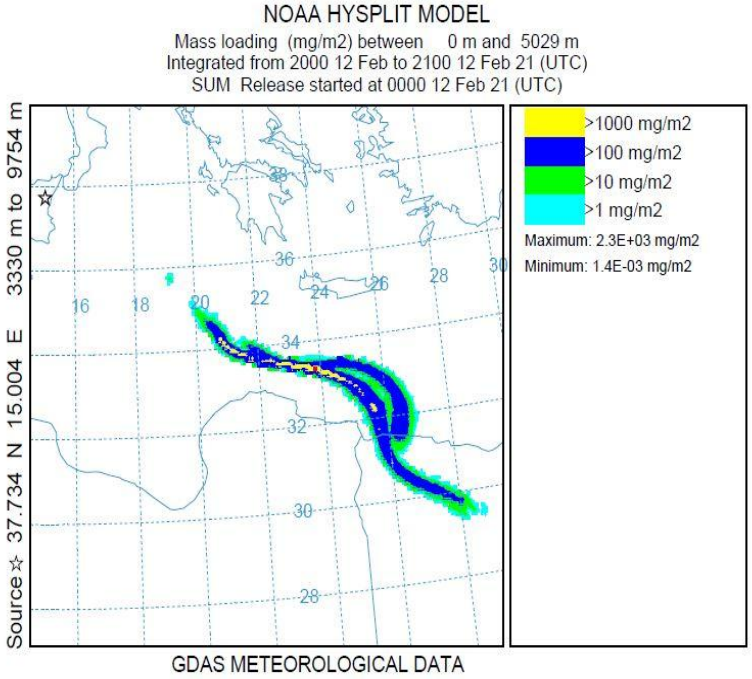

Fig. 68. ash particle concentration in ABL at Mount Etna (12th Feb. 2021) using HYSPLIT modeling system

15th Feb. 2021

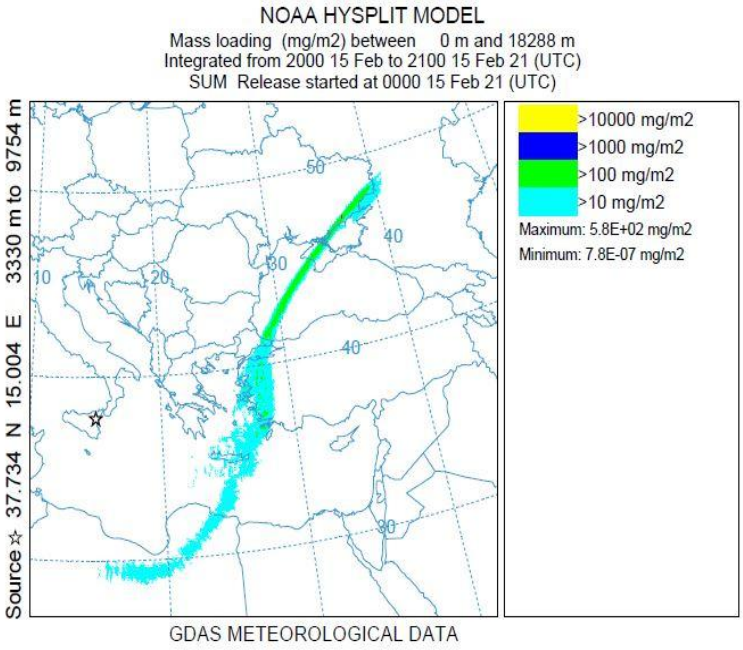

Fig. 69. ash particle concentration in ABL at Mount Etna (15th Feb. 2021) using HYSPLIT modeling system

16th Feb. 2021

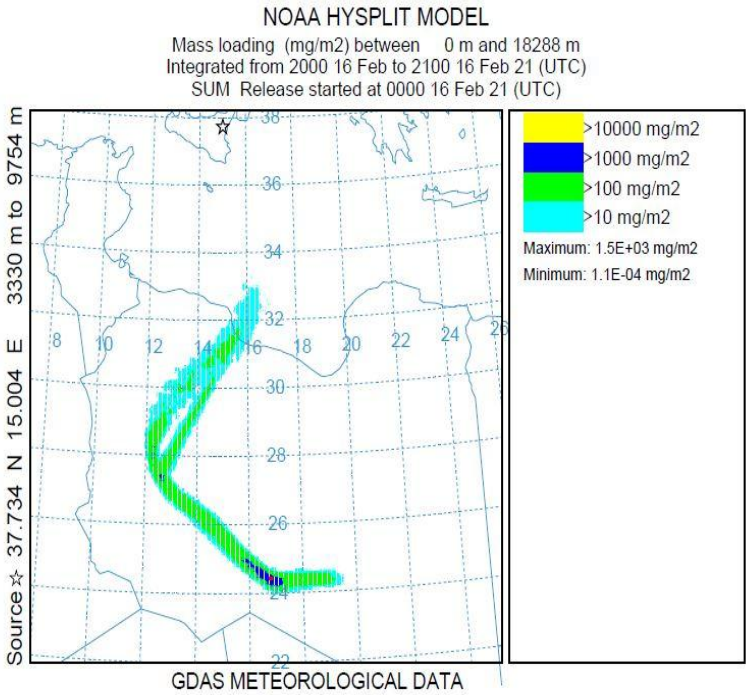

Fig. 70. ash particle concentration in ABL at Mount Etna (16th Feb. 2021) using HYSPLIT modeling system

17th Feb. 2021

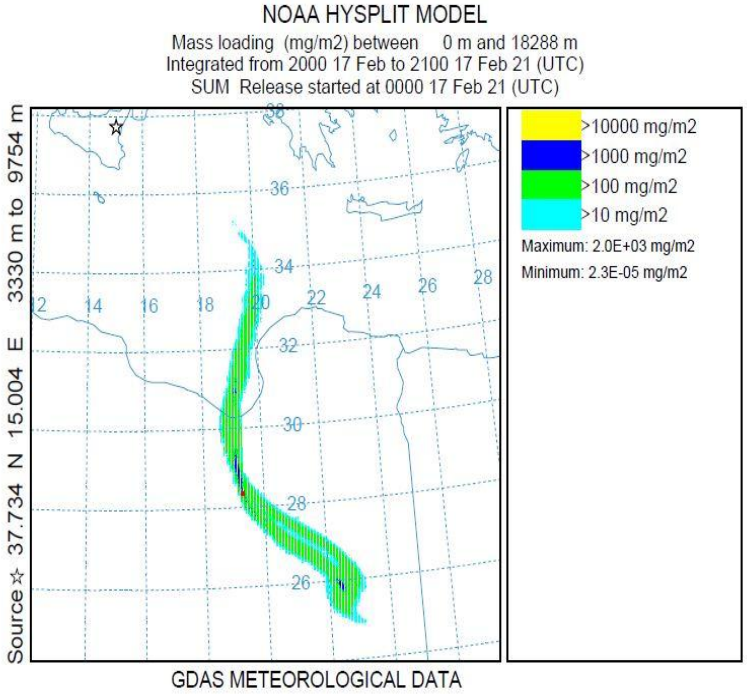

Fig. 71. ash particle concentration in ABL at Mount Etna (17th Feb. 2021) using HYSPLIT modeling system

18th Feb. 2021

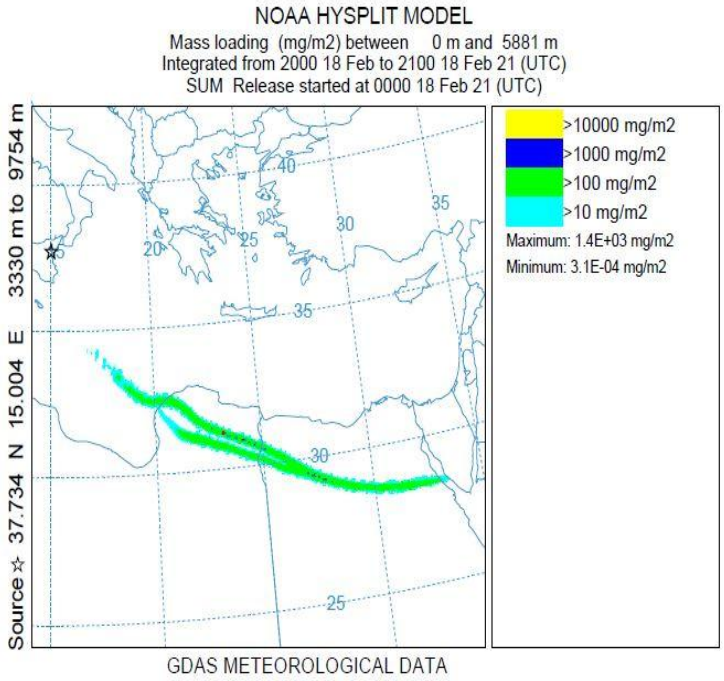

Fig. 72. ash particle concentration in ABL at Mount Etna (18th Feb. 2021) using HYSPLIT modeling system

22nd Feb. 2021

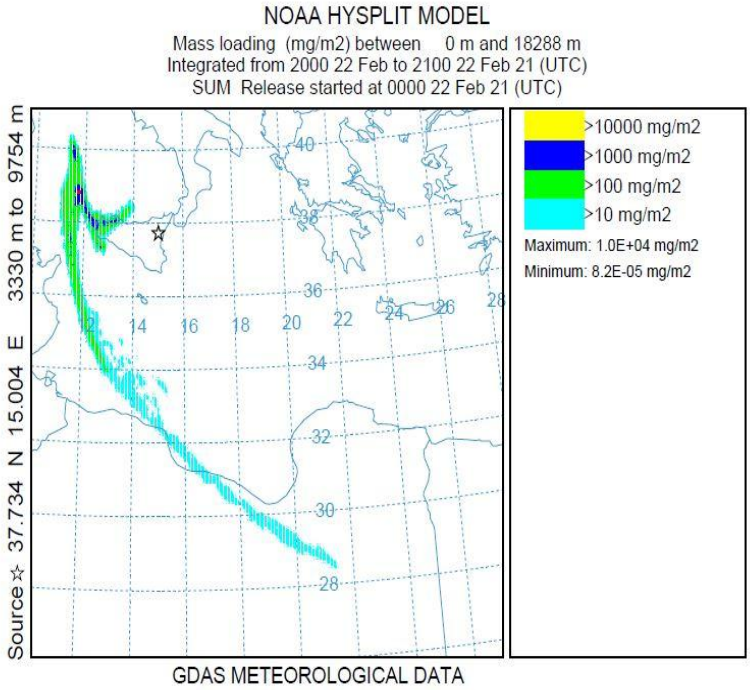

Fig. 73. ash particle concentration in ABL at Mount Etna (22nd Feb. 2021) using HYSPLIT modeling system

28th Feb. 2021

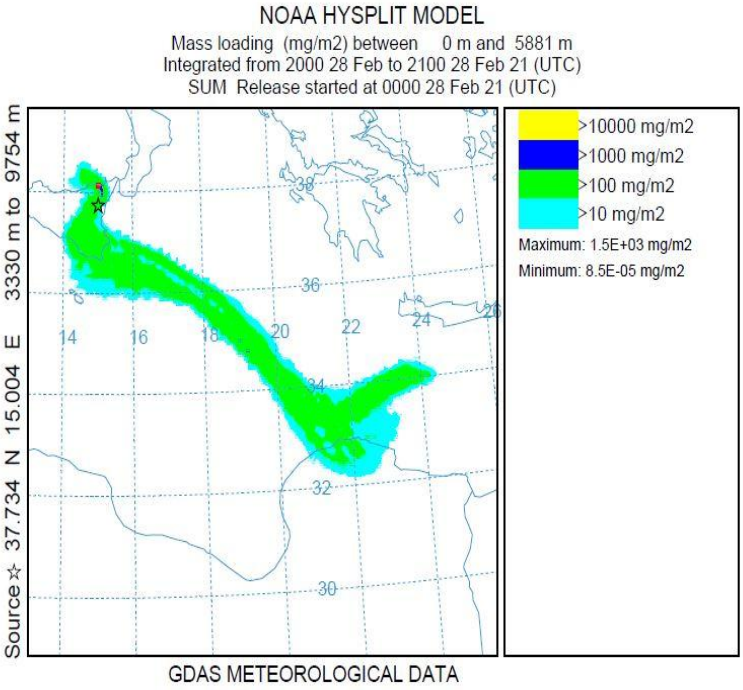

Fig. 74. ash particle concentration in ABL at Mount Etna (28th Feb. 2021) using HYSPLIT modeling system

10th March 2021

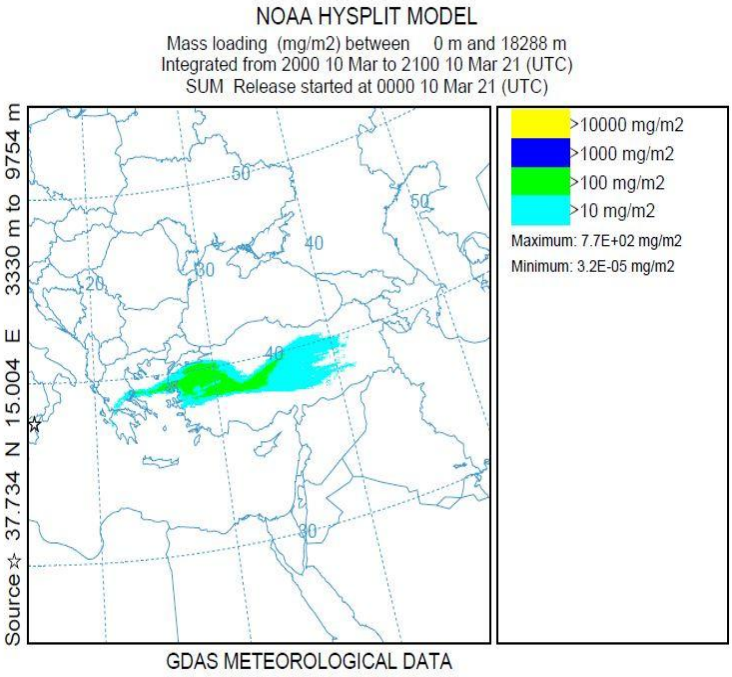

Fig. 75. ash particle concentration in ABL at Mount Etna (10th March 2021) using HYSPLIT modeling system

16th March 2021

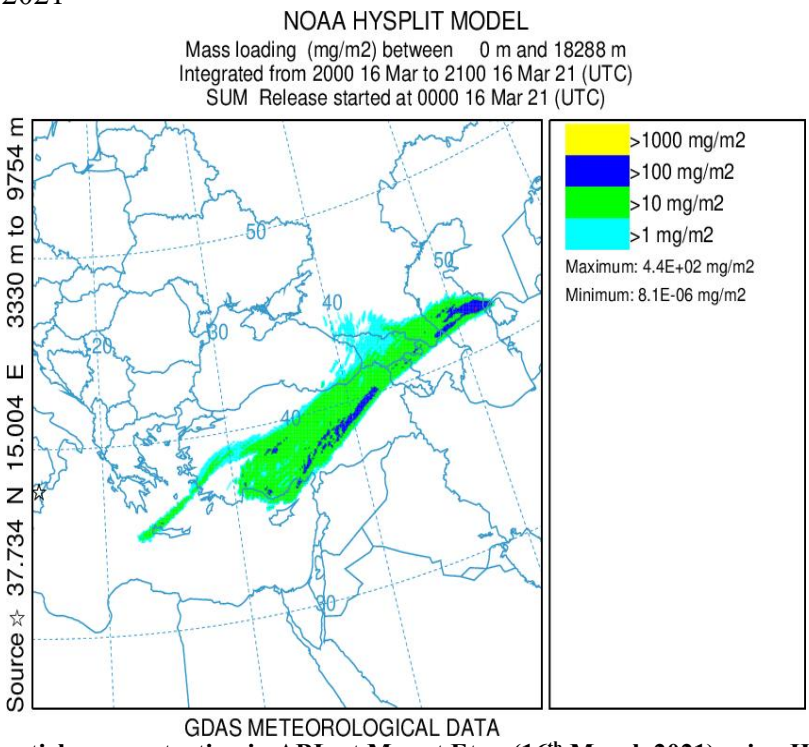

Fig. 76. ash particle concentration in ABL at Mount Etna (16th March 2021) using HYSPLIT modeling system

6. RESULTS AND DISCUSSION

In this section, the simulation results has been analyzed. The simulations estimated using HYSPLIT modelling system has been carried out for Mount Etna volcanic region specially in month of October 2021 and also focusing the eruption month i.e., February 2021. The investigations specifically based on:

- Mass concentration of ash particles
- Ash particle position
- Ash particle deposition

The results from the simulations divided mainly in two parts i.e., with different locations surrounding Mount Etna volcanic region in October 2021 data set and the other part focus on the data set from February 2021 where the eruption occurred on 16th February 2021.

October 2021:
From Fig. 18-27, the volcanic ash concentration during that period has been simulated. The results obtained from different locations of Mount Etna volcanic region. Again from Fig. 28-37, the ash particle position results obtained. The ash particle position in average <6000 m layer (AGL) from all the distinguished simulations where the data set comprises of different locations of Mount Etna. The simulations obtained as test results as the data set varying comprising to the location grid-scale.

February 2021:
Figures 38-50 features volcanic ash particle position simulations of Mount Etna volcano. Fig. 51-63 provides ash particle deposition results of Mount Etna volcano. And, Fig. 64-76 comprises the ash particle concentrations of Mount Etna volcano. In average the ash particle position goes <12000 m layer (AGL) in all the time from the eruption month data set where the eruption happened on 16th February, 2021 where the ash particle deposition occurred at higher rates compare to other simulation as shown in Fig. 58-60 where the deposition level goes >100 mg/m^2 layer. HYSPLIT outputs have more detailed impression of accuracy that's why the large uncertainties in the eruption parameters i.e., the ash particle deposition, ash particle concentration has shown impact as seen in Fig. 70-72, the concentration layer reaches >10000 mg/m^2 which is why the outcome of 16th February 2021 eruption. More than 100,000 volcanic trace particles per day were released during the multiple eruption times of February 2021 month and can be seen from the simulation results from Fig. 38 to 76.

In this thesis, HYSPLIT modelling system for Mount Etna 2021 February month eruptions has been focused and to get clearance reports from the simulations test results the data set of October 2021 too have been simulated in order to make ash forecasting results more visualized. Based on the eruption month simulations HYSPLIT modelling system proves that how monitoring system parameters are in operations and how the forecasting analyzer works with the Mount Etna data set of eruption month and other times.

7. CONCLUSION

This work successfully set up an example regarding the use of HYSPLIT to give forecasts of volcanic ash deposition and ash particle concentrations, with Mount Etna February 2021 (eruption month) and October 2021 data set simulation results. The simulation gives potentially more accurate forecasts using the Lagrangian based simulation modelling system. The volcanic ash concentration and deposition can be successfully forecast model as results shown in eruption month specifically Fig. 70-72 compared to Fig. 24-27. The volcanic ash concentration shows >10000 mg/m^2 in eruption month simulations compared to October 2021 month simulation where the ash concentration level stays at >100 mg/m^2.

The results shows the volcanic eruption of February 16th 2021 plotting with higher mass concentration and dispersal layers of ash particles. The technique focuses in forecasting ash dispersal method in order to evaluate the density that volcanic ash can be depicted in specific space and time during eruption. This thesis deliberates that the methods of improvement in forecasting can be easily analyzed only by improving the monitoring results as provided by NOAA. Advanced modelling like creating special volcanic eruption data set branch in the modelling system with presence of volcanic ash in the air or in the ground can help preventing damages to the eruption area surroundings and airport disruptions. The results also in general gives specification of volcanic risk hazards from volcanic ash, not only estimating the volcanic ash deposition and concentration.

REFERENCES

The 1992 eruptions of crater peak vent, Mount Spurr volcano, Alaska. (1995). https://doi.org/10.3133/b2139

Akaishi, K. (1999). Finding of ancient house buried in lahar deposits generated by the Kemanai pyroclastic flow from Towada volcano, northeastern Japan. *The Journal of the Geological Society of Japan*, *105*(12), XXIII-XXIV. https://doi.org/10.5575/geosoc.105.xxiii

Alam, J. M., & Lin, J. C. (2008). Toward a fully lagrangian atmospheric modeling system. *Monthly Weather Review*, *136*(12), 4653-4667. https://doi.org/10.1175/2008mwr2515.1

Andronico, D., Branca, S., Calvari, S., Burton, M., Caltabiano, T., Corsaro, R. A., Del Carlo, P., Garf, G., Lodato, L., Miraglia, L., Mur, F., Neri, M., Pecora, E., Pompilio, M., Salerno, G., & Spampinato, L. (2004). A multi-disciplinary study of the 2002?03 Etna eruption: Insights into a complex plumbing system. *Bulletin of Volcanology*, *67*(4), 314-330. https://doi.org/10.1007/s00445-004-0372-8

Andronico, D., Cristaldi, A., & Scollo, S. (2008). The 4–5 September 2007 lava fountain at south-east crater of Mt Etna, Italy. *Journal of Volcanology and Geothermal Research*, *173*(3-4), 325-328. https://doi.org/10.1016/j.jvolgeores.2008.02.004

Andronico, D., & Del Carlo, P. (2016). PM10 measurements in urban settlements after lava fountain episodes at Mt. Etna, Italy: Pilot test to assess volcanic ash hazard to human health. *Natural Hazards and Earth System Sciences*, *16*(1), 29-40. https://doi.org/10.5194/nhess-16-29-2016

Andronico, D., Lo Castro, M. D., Sciotto, M., & Spina, L. (2013). The 2010 ash emissions at the summit craters of Mt Etna: Relationship with seismo-acoustic signals. *Journal of Geophysical Research: Solid Earth*, *118*(1), 51-70. https://doi.org/10.1029/2012jb009895

Andronico, D., & Lodato, L. (2005). Effusive activity at Mount Etna volcano (Italy) during the 20th century: A contribution to volcanic hazard assessment. *Natural Hazards*, *36*(3), 407-443. https://doi.org/10.1007/s11069-005-1938-2

Andronico, D., Scollo, S., Caruso, S., & Cristaldi, A. (2008). The 2002–03 Etna explosive activity: Tephra dispersal and features of the deposits. *Journal of Geophysical Research*, *113*(B4). https://doi.org/10.1029/2007jb005126

Andronico, D., Scollo, S., Cristaldi, A., & Ferrari, F. (2009). Monitoring ash emission episodes at Mt. Etna: The 16 November 2006 case study. *Journal of Volcanology and Geothermal Research*, *180*(2-4), 123-134. https://doi.org/10.1016/j.jvolgeores.2008.10.019

Andronico, D., Scollo, S., Cristaldi, A., & Lo Castro, M. D. (2014). Representivity of incompletely sampled fall deposits in estimating eruption source parameters: A test using the 12–13 January 2011 lava fountain deposit from Mt. Etna volcano, Italy. *Bulletin of Volcanology*, *76*(10). https://doi.org/10.1007/s00445-014-0861-3

Andronico, D., Scollo, S., Lo Castro, M. D., Cristaldi, A., Lodato, L., & Taddeucci, J. (2014). Eruption dynamics and tephra dispersal from the 24 November 2006 paroxysm at

south-east crater, Mt Etna, Italy. *Journal of Volcanology and Geothermal Research*, *274*, 78-91. https://doi.org/10.1016/j.jvolgeores.2014.01.009

Andronico, D., Scollo, S., & Cristaldi, A. (2015). Unexpected hazards from tephra fallouts at Mt Etna: The 23 November 2013 lava fountain. *Journal of Volcanology and Geothermal Research*, *304*, 118-125. https://doi.org/10.1016/j.jvolgeores.2015.08.007

Andronico, D., Spinetti, C., Cristaldi, A., & Buongiorno, M. (2009). Observations of Mt. Etna volcanic ash plumes in 2006: An integrated approach from ground-based and polar satellite NOAA–AVHRR monitoring system. *Journal of Volcanology and Geothermal Research*, *180*(2-4), 135-147. https://doi.org/10.1016/j.jvolgeores.2008.11.013

Baldocchi, D., Falge, E., Gu, L., Olson, R., Hollinger, D., Running, S., Anthoni, P., Bernhofer, C., Davis, K., Evans, R., Fuentes, J., Goldstein, A., Katul, G., Law, B., Lee, X., Malhi, Y., Meyers, T., Munger, W., Oechel, W., … Wofsy, S. (2001). Fluxnet: A new tool to study the temporal and spatial variability of ecosystem–scale carbon dioxide, water vapor, and energy flux densities. *Bulletin of the American Meteorological Society*, *82*(11), 2415-2434. https://doi.org/10.1175/1520-0477(2001)0822.3.co;2

Behncke, B., & Neri, M. (2003). Cycles and trends in the recent eruptive behaviour of Mount Etna (Italy). *Canadian Journal of Earth Sciences*, *40*(10), 1405-1411. https://doi.org/10.1139/e03-052

Behncke, B., & Neri, M. (2003). Cycles and trends in the recent eruptive behaviour of Mount Etna (Italy). *Canadian Journal of Earth Sciences*, *40*(10), 1405-1411. https://doi.org/10.1139/e03-052

Behncke, B., Neri, M., & Nagay, A. (2005). Lava flow hazard at Mount Etna (Italy): New data from a GIS-based study. *Kinematics and dynamics of lava flows*. https://doi.org/10.1130/0-8137-2396-5.189

Behncke, B., Neri, M., & Nagay, A. (2005). Lava flow hazard at Mount Etna (Italy): New data from a GIS-based study. *Kinematics and dynamics of lava flows*. https://doi.org/10.1130/0-8137-2396-5.189

Bisson, M., Behncke, B., Fornaciai, A., & Neri, M. (2009). LiDAR-based digital terrain analysis of an area exposed to the risk of lava flow invasion: The Zafferana Etnea territory, Mt. Etna (Italy). *Natural Hazards*, *50*(2), 321-334. https://doi.org/10.1007/s11069-009-9346-7

Bonadonna, C., Ernst, G., & Sparks, R. (1998). Thickness variations and volume estimates of tephra fall deposits: The importance of particle Reynolds number. *Journal of Volcanology and Geothermal Research*, *81*(3-4), 173-187. https://doi.org/10.1016/s0377-0273(98)00007-9

Bonadonna, C., & Houghton, B. F. (2005). Total grain-size distribution and volume of tephra-fall deposits. *Bulletin of Volcanology*, *67*(5), 441-456. https://doi.org/10.1007/s00445-004-0386-2

Branca, S., & Carlo, P. D. (2005). Types of eruptions of Etna volcano AD 1670–2003: Implications for short-term eruptive behaviour. *Bulletin of Volcanology*, *67*(8), 732-742. https://doi.org/10.1007/s00445-005-0412-z

Branca, S., & Del Carlo, P. (2004). Eruptions of Mt. Etna during the past 3,200 years: A revised compilation integrating the historical and stratigraphic records. *Geophysical Monograph Series*, 1-27. https://doi.org/10.1029/143gm02

(1996, November 1). Breaking News, World News and Video from Al Jazeera. https://aljazeera.com

Cappello, A., Bilotta, G., Neri, M., & Negro, C. D. (2013). Probabilistic modeling of future volcanic eruptions at Mount Etna. *Journal of Geophysical Research: Solid Earth*, *118*(5), 1925-1935. https://doi.org/10.1002/jgrb.50190

Cappello, A., Neri, M., Acocella, V., Gallo, G., Vicari, A., & Del Negro, C. (2012). Spatial vent opening probability map of Etna volcano (Sicily, Italy). *Bulletin of Volcanology*, *74*(9), 2083-2094. https://doi.org/10.1007/s00445-012-0647-4

Carey, S. N., & Sigurdsson, H. (1982). Influence of particle aggregation on deposition of distal tephra from the May 18, 1980, eruption of Mount St. Helens volcano. *Journal of Geophysical Research: Solid Earth*, *87*(B8), 7061-7072. https://doi.org/10.1029/jb087ib08p07061

Cassiani, M., Radicchi, A., & Giostra, U. (2005). Probability density function modelling of concentration in and above a canopy layer. *Agricultural and Forest Meteorology*, *133*(1-4), 153-165. https://doi.org/10.1016/j.agrformet.2005.09.007

Cassiani, M., Stohl, A., & Brioude, J. (2014). Lagrangian stochastic modelling of dispersion in the convective boundary layer with skewed turbulence conditions and a vertical density gradient: Formulation and implementation in the FLEXPART model. *Boundary-Layer Meteorology*, *154*(3), 367-390. https://doi.org/10.1007/s10546-014-9976-5

Crisci, G. M., Avolio, M. V., Behncke, B., D'Ambrosio, D., Di Gregorio, S., Lupiano, V., Neri, M., Rongo, R., & Spataro, W. (2010). Predicting the impact of lava flows at Mount Etna, Italy. *Journal of Geophysical Research*, *115*(B4). https://doi.org/10.1029/2009jb006431

Cristina Proietti, Emanuela De Beni, Mauro Coltelli, & Stefano Branca. (2011). The flank eruption history of Etna (1610-2006) as a constraint on lava flow hazard. *Annals of Geophysics*, *54*(5). https://doi.org/10.4401/ag-5333

De Baas, A. F., Van Dop, H., & Nieuwstadt, F. T. (1986). An application of the Langevin equation for inhomogeneous conditions to dispersion in a convective boundary layer. *Quarterly Journal of the Royal Meteorological Society*, *112*(471), 165-180. https://doi.org/10.1002/qj.49711247110

Dosio, A., & De Arellano, J. V. (2006). Statistics of absolute and relative dispersion in the atmospheric convective boundary layer: A large-eddy simulation study. *Journal of the Atmospheric Sciences*, *63*(4), 1253-1272. https://doi.org/10.1175/jas3689.1

Draxler, R., Dietz, R., Lagomarsino, R., & Start, G. (1991). Across North America tracer experiment (ANATEX): Sampling and analysis. *Atmospheric Environment. Part A. General Topics*, *25*(12), 2815-2836. https://doi.org/10.1016/0960-1686(91)90208-o

Draxler, R. R. (1987). Sensitivity of a trajectory model to the spatial and temporal resolution of the meteorological data during CAPTEX. *Journal of Climate and Applied Meteorology*, *26*(11), 1577-1588. https://doi.org/10.1175/1520-0450(1987)0262.0.co;2

Draxler, R. R. (2000). Meteorological factors of ozone predictability at Houston, Texas. *Journal of the Air & Waste Management Association*, *50*(2), 259-271. https://doi.org/10.1080/10473289.2000.10463999

Draxler, R. R. (2003). Evaluation of an ensemble dispersion calculation. *Journal of Applied Meteorology*, *42*(2), 308-317. https://doi.org/10.1175/1520-0450(2003)0422.0.co;2

Draxler, R. R. (2006). The use of global and Mesoscale meteorological model data to predict the transport and dispersion of tracer plumes over Washington, D.C. *Weather and Forecasting*, *21*(3), 383-394. https://doi.org/10.1175/waf926.1

Draxler, R. R. (2007). Demonstration of a global modeling methodology to determine the relative importance of local and long-distance sources. *Atmospheric Environment*, *41*(4), 776-789. https://doi.org/10.1016/j.atmosenv.2006.08.052

Draxler, R. R., & Stunder, B. J. (1988). Modeling the CAPTEX vertical tracer concentration profiles. *Journal of Applied Meteorology*, *27*(5), 617-625. https://doi.org/10.1175/1520-0450(1988)0272.0.co;2

Draxler, R. R., & Taylor, A. D. (1982). Horizontal dispersion parameters for long-range transport modeling. *Journal of Applied Meteorology*, *21*(3), 367-372. https://doi.org/10.1175/1520-0450(1982)0212.0.co;2

Duman, T., Katul, G. G., Siqueira, M. B., & Cassiani, M. (2014). A velocity–dissipation lagrangian stochastic model for turbulent dispersion in atmospheric boundary-layer and canopy flows. *Boundary-Layer Meteorology*, *152*(1), 1-18. https://doi.org/10.1007/s10546-014-9914-6

Duncan, A. M., Chester, D. K., & Guest, J. E. (1981). Mount Etna volcano: Environmental impact and problems of volcanic prediction. *The Geographical Journal*, *147*(2), 164. https://doi.org/10.2307/634532

Escudero, M., Stein, A., Draxler, R. R., Querol, X., Alastuey, A., Castillo, S., & Avila, A. (2006). Determination of the contribution of northern Africa dust source areas to PM10 concentrations over the central Iberian Peninsula using the hybrid single-particle lagrangian integrated trajectory model (HYSPLIT) model. *Journal of Geophysical Research*, *111*(D6). https://doi.org/10.1029/2005jd006395

Farazmand, M., & Haller, G. (2015). The Maxey–Riley equation: Existence, uniqueness and regularity of solutions. *Nonlinear Analysis: Real World Applications*, *22*, 98-106. https://doi.org/10.1016/j.nonrwa.2014.08.002

Fay, B., Glaab, H., Jacobsen, I., & Schrodin, R. (1995). Evaluation of Eulerian and lagrangian atmospheric transport models at the Deutscher Wetterdienst using anatex surface tracer data. *Atmospheric Environment*, *29*(18), 2485-2497. https://doi.org/10.1016/1352-2310(95)00144-n

Gifford, F. (1982). Horizontal diffusion in the atmosphere: A lagrangian-dynamical theory. *Atmospheric Environment (1967)*, *16*(3), 505-512. https://doi.org/10.1016/0004-6981(82)90159-7

Girault, F., Carazzo, G., Tait, S., Ferrucci, F., & Kaminski, É. (2014). The effect of total grain-size distribution on the dynamics of turbulent volcanic plumes. *Earth and Planetary Science Letters*, *394*, 124-134. https://doi.org/10.1016/j.epsl.2014.03.021

Guest, J., Chester, D., & Duncan, A. (1984). The valle del Bove, Mount Etna: Its origin and relation to the stratigraphy and structure of the volcano. *Journal of Volcanology and Geothermal Research*, *21*(1-2), 1-23. https://doi.org/10.1016/0377-0273(84)90013-1

Guest, J. E., & Murray, J. B. (1979). An analysis of hazard from Mount Etna volcano. *Journal of the Geological Society*, *136*(3), 347-354. https://doi.org/10.1144/gsjgs.136.3.0347

Gunn, L. S., Blake, S., Jones, M. C., & Rymer, H. (2013). Forecasting the duration of volcanic eruptions: An empirical probabilistic model. *Bulletin of Volcanology*, *76*(1). https://doi.org/10.1007/s00445-013-0780-8

Harris, A. J., Favalli, M., Wright, R., & Garbeil, H. (2011). Hazard assessment at Mount Etna using a hybrid lava flow Inundation model and satellite-based land classification. *Natural Hazards*, *58*(3), 1001-1027. https://doi.org/10.1007/s11069-010-9709-0

Harris, A., Murray, J., Aries, S., Davies, M., Flynn, L., Wooster, M., Wright, R., & Rothery, D. (2000). Effusion rate trends at Etna and Krafla and their implications for eruptive mechanisms. *Journal of Volcanology and Geothermal Research*, *102*(3-4), 237-269. https://doi.org/10.1016/s0377-0273(00)00190-6

Haszpra, T., & Tél, T. (2011). Volcanic ash in the free atmosphere: A dynamical systems approach. *Journal of Physics: Conference Series*, *333*, 012008. https://doi.org/10.1088/1742-6596/333/1/012008

Heffter, J. L., & Stunder, B. J. (1993). Volcanic ash forecast transport and dispersion (VAFTAD) model. *Weather and Forecasting*, *8*(4), 533-541. https://doi.org/10.1175/1520-0434(1993)0082.0.co;2

Holasek, R. E., Self, S., & Woods, A. W. (1996). Satellite observations and interpretation of the 1991 Mount Pinatubo eruption plumes. *Journal of Geophysical Research: Solid Earth*, *101*(B12), 27635-27655. https://doi.org/10.1029/96jb01179

Holasek, R. E., Self, S., & Woods, A. W. (1996). Satellite observations and interpretation of the 1991 Mount Pinatubo eruption plumes. *Journal of Geophysical Research: Solid Earth*, *101*(B12), 27635-27655. https://doi.org/10.1029/96jb01179

Hsieh, C., Katul, G., & Chi, T. (2000). An approximate analytical model for footprint estimation of scalar fluxes in thermally stratified atmospheric flows. *Advances in Water Resources*, *23*(7), 765-772. https://doi.org/10.1016/s0309-1708(99)00042-1

Hurst, T., & Davis, C. (2017). Forecasting volcanic ash deposition using HYSPLIT. *Journal of Applied Volcanology*, *6*(1). https://doi.org/10.1186/s13617-017-0056-7

Kantha, L., & Clayson, C. (2003). Boundary LAYERS | Ocean mixed layer. *Encyclopedia of Atmospheric Sciences*, 291-298. https://doi.org/10.1016/b0-12-227090-8/00093-2

Kljun, N., Kastner-Klein, P., Fedorovich, E., & Rotach, M. (2004). Evaluation of lagrangian footprint model using data from wind tunnel convective boundary layer. *Agricultural and Forest Meteorology*, *127*(3-4), 189-201. https://doi.org/10.1016/j.agrformet.2004.07.013

Kljun, N., Kormann, R., Rotach, M. W., & Meixer, F. X. (2003). Comparison of the Langrangian footprint. *Boundary-Layer Meteorology*, *106*(2), 349-355. https://doi.org/10.1023/a:1021141223386

Kljun, N., Rotach, M., & Schmid, H. (2002). A three-dimensional backward lagrangian footprint model for a wide range of boundary-layer stratifications. *Boundary-Layer Meteorology*, *103*(2), 205-226. https://doi.org/10.1023/a:1014556300021

Lamb, R. G. (1978). A numerical simulation of dispersion from an elevated point source in the convective planetary boundary layer. *Atmospheric Environment (1967)*, *12*(6-7), 1297-1304. https://doi.org/10.1016/0004-6981(78)90068-9

Luhar, A. K., & Britter, R. E. (1989). A random walk model for dispersion in inhomogeneous turbulence in a convective boundary layer. *Atmospheric Environment (1967)*, *23*(9), 1911-1924. https://doi.org/10.1016/0004-6981(89)90516-7

Maeno, F., Nagai, M., Nakada, S., Burden, R. E., Engwell, S., Suzuki, Y., & Kaneko, T. (2014). Constraining tephra dispersion and deposition from three subplinian explosions in 2011 at Shinmoedake volcano, Kyushu, Japan. *Bulletin of Volcanology*, *76*(6). https://doi.org/10.1007/s00445-014-0823-9

Marco Neri, Valerio Acocella, Boris Behncke, Salvatore Giammanco, Francesco Mazzarini, & Derek Rust. (2011). Structural analysis of the eruptive fissures at Mount Etna (Italy). *Annals of Geophysics*, *54*(5). https://doi.org/10.4401/ag-5332

Marco Sampaolo. (2013, May 7). *Mount Etna*. Encyclopedia Britannica. https://www.britannica.com/place/Mount-Etna

Moeng, C., & Wyngaard, J. C. (1988). Spectral analysis of large-eddy simulations of the convective boundary layer. *Journal of the Atmospheric Sciences*, *45*(23), 3573-3587. https://doi.org/10.1175/1520-0469(1988)0452.0.co;2

Mount Etna and the 1971 eruption - The 1971 Etna eruption: Petrography of the lavas. (1973). *Philosophical Transactions of the Royal Society of London. Series A, Mathematical and Physical Sciences*, *274*(1238), 45-53. https://doi.org/10.1098/rsta.1973.0024

Mount Etna and the 1971 eruption - The 1971 Etna eruption: Petrography of the lavas. (1973). *Philosophical Transactions of the Royal Society of London. Series A, Mathematical and Physical Sciences*, *274*(1238), 45-53. https://doi.org/10.1098/rsta.1973.0024

Mulargia, F., Tinti, S., & Boschi, E. (1985). A statistical analysis of flank eruptions on Etna volcano. *Journal of Volcanology and Geothermal Research*, *23*(3-4), 263-272. https://doi.org/10.1016/0377-0273(85)90037-x

Nathan, R., Katul, G. G., Horn, H. S., Thomas, S. M., Oren, R., Avissar, R., Pacala, S. W., & Levin, S. A. (2002). Mechanisms of long-distance dispersal of seeds by wind. *Nature*, *418*(6896), 409-413. https://doi.org/10.1038/nature00844

National Institute of Geophysics and Volcanology, Catania section, Etneo Observatory. (1999). https://www.ct.ingv.it/

Neri, M., & Acocella, V. (2006). The 2004–2005 Etna eruption: Implications for flank deformation and structural behaviour of the volcano. *Journal of Volcanology and Geothermal Research*, *158*(1-2), 195-206. https://doi.org/10.1016/j.jvolgeores.2006.04.022

Passarelli, L., Sansò, B., Sandri, L., & Marzocchi, W. (2010). Testing forecasts of a new Bayesian time-predictable model of eruption occurrence. *Journal of Volcanology and Geothermal Research*, *198*(1-2), 57-75. https://doi.org/10.1016/j.jvolgeores.2010.08.011

Peterson, R., Webley, P., D'Amours, R., Servranckx, R., Stunder, B., & Papp, K. (2015). Volcanic ash transport and dispersion models. *Monitoring Volcanoes in the North Pacific*, 187-233. https://doi.org/10.1007/978-3-540-68750-4_7

Plu, M., Bigeard, G., Sič, B., Emili, E., Bugliaro, L., El Amraoui, L., Guth, J., Josse, B., Mona, L., & Piontek, D. (2021). Modelling the volcanic ash plume from Eyjafjallajökull eruption (May 2010) over Europe: Evaluation of the benefit of source term improvements and of the assimilation of aerosol measurements. *Natural Hazards and Earth System Sciences*, *21*(12), 3731-3747. https://doi.org/10.5194/nhess-21-3731-2021

Poggi, D., Katul, G., & Albertson, J. (2006). Scalar dispersion within a model canopy: Measurements and three-dimensional lagrangian models. *Advances in Water Resources*, *29*(2), 326-335. https://doi.org/10.1016/j.advwatres.2004.12.017

Pope, S. B. (2000). Turbulent flows. https://doi.org/10.1017/cbo9780511840531

Pope, S. B., & Chen, Y. L. (1990). The velocity-dissipation probability density function model for turbulent flows. *Physics of Fluids A: Fluid Dynamics*, *2*(8), 1437-1449. https://doi.org/10.1063/1.857592

Pope, S. B., & Chen, Y. L. (1990). The velocity-dissipation probability density function model for turbulent flows. *Physics of Fluids A: Fluid Dynamics*, *2*(8), 1437-1449. https://doi.org/10.1063/1.857592

Pyle, D. (1998). Sparks, R. S. J., BURSIK, M. I., Carey, S. N., Gilbert, J. S., glaze, L. S., SIGURDSSON, H. & woods, A. W. 1997. Volcanic plumes. xv + 574 pp. Chichester, New York, Weinheim, Brisbane, Singapore, Toronto: John Wiley & Sons. Price £85.00 (hard covers). Isbn 0 471 93901 3. *Geological Magazine*, *135*(1), 143-158. https://doi.org/10.1017/s0016756897278258

Ram, M., & Gayley, R. I. (1991). Long-range transport of volcanic ash to the Greenland ice sheet. *Nature*, *349*(6308), 401-404. https://doi.org/10.1038/349401a0

Rannik, Ü., Aubinet, M., Kurbanmuradov, O., Sabelfeld, K. K., Markkanen, T., & Vesala, T. (2000). Footprint analysis for measurements over a heterogeneous forest. *Boundary-Layer Meteorology*, *97*(1), 137-166. https://doi.org/10.1023/a:1002702810929

Rannik, Ü., Markkanen, T., Raittila, J., Hari, P., & Vesala, T. (2003). Turbulence statistics inside and over forest: Influence on footprint prediction. *Boundary-Layer Meteorology*, *109*(2), 163-189. https://doi.org/10.1023/a:1025404923169

Reynolds, A. M. (2018). Incorporating terminal velocities into lagrangian stochastic models of particle dispersal in the atmospheric boundary layer. *Scientific Reports*, *8*(1). https://doi.org/10.1038/s41598-018-34924-4

Rose, W., & Durant, A. (2009). Fine ash content of explosive eruptions. *Journal of Volcanology and Geothermal Research*, *186*(1-2), 32-39. https://doi.org/10.1016/j.jvolgeores.2009.01.010

Rose, W. I. (1993). Comment on ?another look at the calculation of fallout tephra volumes? by Judy Fierstein and Manuel Nathenson. *Bulletin of Volcanology*, *55*(5), 372-374. https://doi.org/10.1007/bf00301148

Rose, W. I., Anderson, A. T., Woodruff, L. G., & Bonis, S. B. (1978). The October 1974 basaltic tephra from fuego volcano: Description and history of the magma body. *Journal of Volcanology and Geothermal Research*, *4*(1-2), 3-53. https://doi.org/10.1016/0377-0273(78)90027-6

Rose, W. I., Delene, D. J., Schneider, D. J., Bluth, G. J., Krueger, A. J., Sprod, I., McKee, C., Davies, H. L., & Ernst, G. G. (1995). Ice in the 1994 Rabaul eruption cloud: Implications for volcano hazard and atmospheric effects. *Nature*, *375*(6531), 477-479. https://doi.org/10.1038/375477a0

Rose, W. I., Self, S., Murrow, P. J., Bonadonna, C., Durant, A. J., & Ernst, G. G. (2007). Nature and significance of small volume fall deposits at composite volcanoes: Insights from the October 14, 1974 fuego eruption, Guatemala. *Bulletin of Volcanology*, *70*(9), 1043-1067. https://doi.org/10.1007/s00445-007-0187-5

Salvi, F., Scandone, R., & Palma, C. (2006). Statistical analysis of the historical activity of Mount Etna, aimed at the evaluation of volcanic hazard. *Journal of Volcanology and Geothermal Research*, *154*(3-4), 159-168. https://doi.org/10.1016/j.jvolgeores.2006.01.002

Sawford, B. L., & Guest, F. M. (1987). Lagrangian stochastic analysis of flux-gradient relationships in the convective boundary layer. *Journal of the Atmospheric Sciences*, *44*(8), 1152-1165. https://doi.org/10.1175/1520-0469(1987)0442.0.co;2

Shao, Y. (1992). Turbulent dispersion in coastal atmospheric boundary layers: An application of a lagrangian model. *Boundary-Layer Meteorology*, *59*(4), 363-385. https://doi.org/10.1007/bf02215459

Smethurst, L., James, M. R., Pinkerton, H., & Tawn, J. A. (2009). A statistical analysis of eruptive activity on Mount Etna, Sicily. *Geophysical Journal International*, *179*(1), 655-666. https://doi.org/10.1111/j.1365-246x.2009.04286.x

Stein, A. F., Draxler, R. R., Rolph, G. D., Stunder, B. J., Cohen, M. D., & Ngan, F. (2015). NOAA's HYSPLIT atmospheric transport and dispersion modeling system. *Bulletin of the American Meteorological Society*, *96*(12), 2059-2077. https://doi.org/10.1175/bams-d-14-00110.1

SULLIVAN, P. P., HORST, T. W., LENSCHOW, D. H., MOENG, C., & WEIL, J. C. (2003). Structure of subfilter-scale fluxes in the atmospheric surface layer with application to

large-eddy simulation modelling. *Journal of Fluid Mechanics*, *482*, 101-139. https://doi.org/10.1017/s0022112003004099

Suzuki, Y. J. (2005). A numerical study of turbulent mixing in eruption clouds using a three-dimensional fluid dynamics model. *Journal of Geophysical Research*, *110*(B8). https://doi.org/10.1029/2004jb003460

Suzuki, Y. J., & Koyaguchi, T. (2009). A three-dimensional numerical simulation of spreading umbrella clouds. *Journal of Geophysical Research*, *114*(B3). https://doi.org/10.1029/2007jb005369

Taddeucci, J., Pompilio, M., & Scarlato, P. (2002). Monitoring the explosive activity of the July-August 2001 eruption of Mt. Etna (Italy) by ash characterization. *Geophysical Research Letters*, *29*(8), 71-1-71-4. https://doi.org/10.1029/2001gl014372

Taddeucci, J., Pompilio, M., & Scarlato, P. (2004). Conduit processes during the July–August 2001 explosive activity of Mt. Etna (Italy): Inferences from glass chemistry and crystal size distribution of ash particles. *Journal of Volcanology and Geothermal Research*, *137*(1-3), 33-54. https://doi.org/10.1016/j.jvolgeores.2004.05.011

Talbot, J. P., Self, S., & Wilson, C. J. (1994). Dilute gravity current and rain-flushed ash deposits in the 1.8 Ka Hatepe Plinian deposit, Taupo, New Zealand. *Bulletin of Volcanology*, *56*(6-7), 538-551. https://doi.org/10.1007/bf00302834

Tanguy, J. C. (1981). Les eruptions Historiques de L'Etna: Chronologie et localisation. *Bulletin Volcanologique*, *44*(3), 585-640. https://doi.org/10.1007/bf02600588

Tanguy, J., Condomines, M., Le Goff, M., Chillemi, V., La Delfa, S., & Patanè, G. (2007). Mount Etna eruptions of the last 2,750 years: Revised chronology and location through archeomagnetic and 226Ra-230Th dating. *Bulletin of Volcanology*, *70*(1), 55-83. https://doi.org/10.1007/s00445-007-0121-x

Tanguy, J., Le Goff, M., Principe, C., Arrighi, S., Chillemi, V., Paiotti, A., La Delfa, S., & Patanè, G. (2003). Archeomagnetic dating of Mediterranean volcanics of the last 2100

years: Validity and limits. *Earth and Planetary Science Letters*, *211*(1-2), 111-124. https://doi.org/10.1016/s0012-821x(03)00186-9

Taylor, G. I. (1922). Diffusion by continuous movements. *Proceedings of the London Mathematical Society*, *s2-20*(1), 196-212. https://doi.org/10.1112/plms/s2-20.1.196

Thomson, D. J. (1984). Random walk modelling of diffusion in inhomogeneous turbulence. *Quarterly Journal of the Royal Meteorological Society*, *110*(466), 1107-1120. https://doi.org/10.1002/qj.49711046620

Thomson, D. J. (1987). Criteria for the selection of stochastic models of particle trajectories in turbulent flows. *Journal of Fluid Mechanics*, *180*(-1), 529. https://doi.org/10.1017/s0022112087001940

Vesala, T., Kljun, N., Rannik, Ü., Rinne, J., Sogachev, A., Markkanen, T., Sabelfeld, K., Foken, T., & Leclerc, M. (2008). Flux and concentration footprint modelling: State of the art. *Environmental Pollution*, *152*(3), 653-666. https://doi.org/10.1016/j.envpol.2007.06.070

Walker, G. (1980). The Taupo pumice: Product of the most powerful known (ultraplinian) eruption? *Journal of Volcanology and Geothermal Research*, *8*(1), 69-94. https://doi.org/10.1016/0377-0273(80)90008-6

Walker, G. P. (1981). Characteristics of two phreatoplinian ashes, and their water-flushed origin. *Journal of Volcanology and Geothermal Research*, *9*(4), 395-407. https://doi.org/10.1016/0377-0273(81)90046-9

Walker, G. P. (1981). Plinian eruptions and their products. *Bulletin Volcanologique*, *44*(3), 223-240. https://doi.org/10.1007/bf02600561

WALKER, G. P., & CROASDALE, R. (1971). Two plinian-type eruptions in the Azores. *Journal of the Geological Society*, *127*(1), 17-55. https://doi.org/10.1144/gsjgs.127.1.0017

Walker, G. P., Self, S., & Wilson, L. (1984). Tarawera 1886, New Zealand — A basaltic plinian fissure eruption. *Journal of Volcanology and Geothermal Research*, *21*(1-2), 61-78. https://doi.org/10.1016/0377-0273(84)90016-7

Webley, P., Dehn, J., Lovick, J., Dean, K., Bailey, J., & Valcic, L. (2009). Near-real-time volcanic ash cloud detection: Experiences from the Alaska volcano observatory. *Journal of Volcanology and Geothermal Research*, *186*(1-2), 79-90. https://doi.org/10.1016/j.jvolgeores.2009.02.010

Webley, P., & Mastin, L. (2009). Improved prediction and tracking of volcanic ash clouds. *Journal of Volcanology and Geothermal Research*, *186*(1-2), 1-9. https://doi.org/10.1016/j.jvolgeores.2008.10.022

Webley, P., Stunder, B., & Dean, K. (2009). Preliminary sensitivity study of eruption source parameters for operational volcanic ash cloud transport and dispersion models — A case study of the August 1992 eruption of the crater peak vent, Mount Spurr, Alaska. *Journal of Volcanology and Geothermal Research*, *186*(1-2), 108-119. https://doi.org/10.1016/j.jvolgeores.2009.02.012

Webley, P. W., Dean, K. G., Dehn, J., Bailey, J. E., & Peterson, R. (2010). Volcanic-ash dispersion modeling of the 2006 eruption of Augustine volcano using the puff model: Chapter 21 in *The 2006 eruption of Augustine volcano, Alaska*. *Professional Paper*, 507-526. https://doi.org/10.3133/pp176921

Webley, P. W., Dean, K. G., Dehn, J., Bailey, J. E., & Peterson, R. (2010). Volcanic-ash dispersion modeling of the 2006 eruption of Augustine volcano using the puff model: Chapter 21 in *The 2006 eruption of Augustine volcano, Alaska*. *Professional Paper*, 507-526. https://doi.org/10.3133/pp176921

Willis, G., & Deardorff, J. (1978). A laboratory study of dispersion from an elevated source within a modeled convective planetary boundary layer. *Atmospheric Environment (1967)*, *12*(6-7), 1305-1311. https://doi.org/10.1016/0004-6981(78)90069-0

Willis, G. E., & Deardorff, J. W. (1976). A laboratory model of diffusion into the convective planetary boundary layer. *Quarterly Journal of the Royal Meteorological Society*, *102*(432), 427-445. https://doi.org/10.1002/qj.49710243212

Wilson, J. D. (1988). A second-order closure model for flow through vegetation. *Boundary-Layer Meteorology*, *42*(4), 371-392. https://doi.org/10.1007/bf00121591

Wilson, J. D., & Flesch, T. K. (1993). Flow boundaries in random-flight dispersion models: Enforcing the well-mixed condition. *Journal of Applied Meteorology*, *32*(11), 1695-1707. https://doi.org/10.1175/1520-0450(1993)0322.0.co;2

Wilson, J. D., & Sawford, B. L. (1996). Review of lagrangian stochastic models for trajectories in the turbulent atmosphere. *Boundary-Layer Meteorology 25th Anniversary Volume, 1970–1995*, 191-210. https://doi.org/10.1007/978-94-017-0944-6_9

Woods, A. W. (1993). Moist convection and the injection of volcanic ash into the atmosphere. *Journal of Geophysical Research: Solid Earth*, *98*(B10), 17627-17636. https://doi.org/10.1029/93jb00718

Woods, A. W., & Bursik, M. I. (1991). Particle fallout, thermal disequilibrium and volcanic plumes. *Bulletin of Volcanology*, *53*(7), 559-570. https://doi.org/10.1007/bf00298156

Woods, A. W., & Self, S. (1992). Thermal disequilibrium at the top of volcanic clouds and its effect on estimates of the column height. *Nature*, *355*(6361), 628-630. https://doi.org/10.1038/355628a0

National Institute of Geophysics and Volcanology, Catania section, Etneo Observatory. (1999). https://www.ct.ingv.it/

First post. https://www.firstpost.com/world/sicilians-not-worried-that-mount-etna-is-erupting-as-they-have-seen-worse-9313981.html

Scollo, S., Prestifilippo, M., Spata, G., D' Agostino, M., & Coltelli, M. Monitoring and forecasting Etna volcanic plumes. *NaNat. Hazards Earth Syst. Sci.*, 9, 1573-1585, 2009. https://www.nat-hazards-earth-syst-sci.net/9/1573/2009/